Cell-surface phosphatidylserine regulates osteoclast precursor fusion

Received for publication, August 1, 2017, and in revised form, November 2, 2017 Published, Papers in Press, November 3, 2017, DOI 10.1074/jbc.M117.809681

Santosh K. Verma[‡], Evgenia Leikina[‡], Kamran Melikov[‡], Claudia Gebert[§], Vardit Kram[¶], Marian F. Young[¶], Berna Uygur[‡], and Leonid V. Chernomordik[‡1]

From the Sections on [‡]Membrane Biology and [§]Genomic Imprinting, Eunice Kennedy Shriver NICHD, and [¶]Craniofacial and Skeletal Diseases Branch, NIDCR, National Institutes of Health, Bethesda, Maryland 20892

Edited by Xiao-Fan Wang

Bone-resorbing multinucleated osteoclasts that play a central role in the maintenance and repair of our bones are formed from bone marrow myeloid progenitor cells by a complex differentiation process that culminates in fusion of mononuclear osteoclast precursors. In this study, we uncoupled the cell fusion step from both pre-fusion stages of osteoclastogenic differentiation and the post-fusion expansion of the nascent fusion connections. We accumulated ready-to-fuse cells in the presence of the fusion inhibitor lysophosphatidylcholine and then removed the inhibitor to study synchronized cell fusion. We found that osteoclast fusion required the dendrocyte-expressed seven transmembrane protein (DC-STAMP)-dependent non-apoptotic exposure of phosphatidylserine at the surface of fusion-committed cells. Fusion also depended on extracellular annexins, phosphatidylserine-binding proteins, which, along with annexin-binding protein S100A4, regulated fusogenic activity of syncytin 1. Thus, in contrast to fusion processes mediated by a single protein, such as epithelial cell fusion in *Caenorhabditis elegans*, the cell fusion step in osteoclastogenesis is controlled by phosphatidylserine-regulated activity of several proteins.

The molecular dissection of the best-characterized virus–cell membrane fusion and intracellular fusion processes has been greatly facilitated by their relative rapidity (taking from a few milliseconds to minutes) and by convenient triggers (such as calcium ions, acidification, and receptor interaction) (1–4). Much less is known about mechanisms of cell–cell fusion in fertilization, in development and regeneration of skeletal muscles, in placentogenesis, and in osteoclast formation (3, 5). In all these cell fusion processes, actual fusion events follow relatively slow (days) and unsynchronized pre-fusion stages. To identify the proteins that mediate cell fusion, one needs to distinguish these proteins from proteins that function only in the pre-fusion stages of osteoclastogenesis. Moreover, because cell–cell fusion is usually scored as formation of multinucleated cells, the candidate proteins can operate at a stage where two membranes are already fused and nascent fusion pores expand to fully join the cells (6, 7).

Different cell–cell fusions involve very different proteins and cells and take place in very different biological contexts (2, 3, 8). Although the processes that commit the cells to fusion are likely to be as diverse as the cells involved, fusion events in many cell–cell fusions appear to share some important mechanistic motifs. To start, diverse cell–cell fusions, like many other membrane fusion processes, proceed via hemifusion intermediates (9). Myoblast fusion (7), osteoclast fusion (6), and fusion between epithelial cells in *Caenorhabditis elegans* (10) are all inhibited by the same lipid, lysophosphatidylcholine (LPC),[2] that blocks early hemifusion intermediates (9). Downstream of the apparently conserved membrane rearrangements that generate fusion pores (9), the expansion of these pores to fully join the cells in different cell–cell fusion processes shares dependence on cell metabolism and dynamin 2 activity (6, 7).

In another striking similarity, macrophages committed to fuse into inflammatory giant cells (11), myoblasts committed to fuse into myotubes (12), and trophoblasts committed to form placental syncytiotrophoblasts (13) have all been reported to expose phosphatidylserine (PS) at the cell surface. Reports that cell-surface PS influences differentiation processes for both myoblasts (14) and osteoclasts (15) implicate PS exposure in pre-fusion stages. However, the dependence of myoblast fusion on extracellular PS-binding proteins, annexins A1 and A5 (Anxs A1 and A5) (7, 16, 17) and stabilin 2 (18), suggests that cell-surface PS may be involved in myoblast fusion.

In this study, we focused on the cell–cell fusion stage of osteoclast formation (19, 20). Multinucleated osteoclasts resorb bones to balance the bone-forming activity of osteoblasts in the continuous bone-remodeling process in both healthy animals and in pathological states. Osteoclasts are formed from precursor cells (OCPs) of monocyte/macrophage lineage in the presence of macrophage colony-stimulating factor (M-CSF) and receptor activator of NF-κB ligand (RANKL). Many groups

This work was supported by the Intramural Research Program of the Eunice Kennedy Shriver NICHD, National Institutes of Health (to the L. V. C. laboratory), and by the NIDCR, National Institutes of Health (to the M. F. Y. laboratory). The authors declare that they have no conflicts of interest with the contents of this article. The content is solely the responsibility of the authors and does not necessarily represent the official views of the National Institutes of Health.
This article contains Figs. S1–S6.

[1] To whom correspondence should be addressed. Tel.: 301-594-1128; Fax: 301-480-2916; E-mail: chernoml@mail.nih.gov.

[2] The abbreviations used are: LPC, lysophosphatidylcholine; Anx, annexin; BMC, bone marrow cell; HM, human monocyte; M-CSF, macrophage colony-stimulating factor; PS, phosphatidylserine; RANK, receptor activator of nuclear factor-κB; RANKL, receptor activator of nuclear factor-κB ligand; OCP, osteoclast precursor cell; TRAP, tartrate-resistant acidic phosphatase; MEM-α, minimal essential medium-α; CDF, cumulative distribution function; DiI, 1,1′-dioctadecyl-3,3,3′,3′-tetramethylindocarbocyanine perchlorate.

have characterized the osteoclastogenesis using *in vitro* models based on human monocytes (HMs), murine bone marrow cells (BMC), and macrophage-like murine monocytic RAW 264.7 cells ("RAW cells"). Several proteins have been shown to be involved in osteoclastogenesis and suggested to be involved in OCP fusion, including the following: a regulator of immune properties of dendritic cells, dendritic cell-specific transmembrane protein (DC-STAMP) (21, 22); osteoclast stimulatory transmembrane protein (OC-STAMP) (23, 24); purinergic receptors (25); S100 proteins (26); protein-tyrosine phosphatase PEST (27); adaptor protein Tks5 (28); an intermediate-conductance calcium-activated potassium channel (29); and CD47 (30). Recent studies have also demonstrated that formation of multinucleated osteoclasts depends on clathrin-mediated endocytosis (31). The specific stages of osteoclastogenesis that are dependent on the proteins listed above (fusion *versus* pre- or post-fusion stages) remain to be clarified.

Generation of multinucleated osteoclasts also involves syncytin-1 (Syn-1), the envelope protein of a human endogenous retrovirus, HERVW1 (30, 32, 33). Syn-1 is highly expressed in placental trophoblasts and mediates their fusion in human placentogenesis (34). Fusogenic activity of Syn-1 is triggered by its interactions with ASCT1/2 receptors. Suppression of Syn-1 activity inhibits both formation of multinucleated human osteoclasts and expression of a biochemical marker of osteoclast maturation, tartrate-resistant acidic phosphatase (TRAP) (32). Because TRAP expression develops independently of cell–cell fusion (6, 21), these findings suggest that Syn-1 either functions in both the fusion stage and the pre-fusion stages leading to TRAP expression or only in the differentiation stages upstream of both TRAP expression and fusion. Indeed, Syn-1 has been reported to have non-fusion-related functions (35).

Proteins found to be required for formation of multinucleated osteoclasts, especially those among them that are not required for expression of some osteoclast differentiation markers, are routinely referred to as proteins involved in fusion. However, distinguishing proteins that are required for generation of ready-to-fuse OCPs from proteins that are directly involved in fusion has remained a challenge because all proteins discussed above have known fusion-unrelated functions. Here, we explored mechanisms of the cell fusion stage in osteoclastogenesis using murine OCPs (macrophage-like cells and BMCs) and HM-derived OCPs. To distinguish an actual fusion event, *i.e.* a local merger between cell membranes from post-fusion expansion of nascent fusion connections, we complemented the conventional syncytium formation assay with an assay that detected fusion as redistribution of small probes. To uncouple the fusion stage from the pre-fusion stages, we used the fusion-synchronization approach that we developed earlier to study the post-fusion stage of osteoclastogenesis when the connection between two OCPs expands to form syncytium (6). We accumulated the ready-to-fuse OCPs in the presence of fusion inhibitor LPC and then removed LPC to ensue robust fusion. This approach has allowed us to specifically study ready-to-fuse and fusing cells. Application of different reagents at the time of LPC removal allowed us to examine contributions of candidate proteins to osteoclast fusion.

We found that fusion-committed OCPs displayed PS at their surface, and this PS exposure depended on DC-STAMP and was required for fusion, suggesting involvement of extracellular PS-binding proteins. Indeed, we found that synchronized fusion depends on extracellular Anxs (A1 and A5 for murine osteoclasts and only A5 for HM-derived OCPs). Synchronized fusion of HM-derived OCPs also involved Anx-binding protein S100A4 and Syn-1. Our data substantiate a novel mechanism of osteoclast fusion in which DC-STAMP-dependent phosphatidylserine exposure triggers the assembly of the annexin-based protein scaffold that regulates fusogenic activity of Syn-1. The dependence of the cell fusion stage of osteoclastogenesis on the interdependent activities of the Anxs and Syn-1 can be shared by other cell–cell fusion processes.

Results

Fusion synchronization

We have previously analyzed the time course of formation of multinucleated osteoclasts for RAW cells and for HM-derived OCPs and, in each of these models, selected the 16-h intervals characterized by the most robust fusion (6). For both the RAW cells and HM-derived OCPs, we focused on fusion observed between 72 and 88 h post-RANKL application. Conventionally, osteoclast fusion is quantified from measurements of numbers and sizes (area and number of nuclei) of multinucleated cells. These syncytium formation assays detect only fusion events with fully expanded fusion pores. Because some treatments block the expansion of nascent fusion pores rather than the actual fusion event that generates these pores (6, 7), we complemented syncytium formation assays with an assay for local membrane merger, defined as a connection between two cell membranes. In this assay, we co-incubated the cells labeled with cytosolic green cell tracker and cells labeled with either red membrane probe 1,1′-dioctadecyl-3,3,3′,3′-tetramethylindocarbocyanine perchlorate (DiI) or cytosolic orange cell tracker and counted syncytia co-labeled with both green and red probes. We have not aimed to distinguish hemifusion (= only lipid mixing) from fusion pores (= both lipid and content mixing), and we considered appearance of any double-labeled cells as evidence of membrane merger.

As illustrated in Fig. 1, *left panel,* LPC application at the beginning of the selected time interval suppressed both membrane merger and syncytium formation. 16 h later, we washed the cells with LPC-free medium to allow fusion. For HM-derived OCPs, the extents of membrane merger (*B*) and the numbers of completed fusion events (*C*) grew from the background levels that reflected the fusion levels observed at the time of LPC application (Fig. 1, *A–D*). Within 90 min after LPC removal, the membrane merger and syncytium formation extents were close to those observed at the same time post-RANKL application in the control experiments with no LPC applied (Fig. 1, *B* and *C*). Analysis of the distributions of the sizes of syncytia presented as cumulative distribution function (CDF) (Fig. 1*D*) confirmed that LPC inhibited growth of syncytia, and 90 min after LPC removal, the numbers of syncytia of different sizes were close to those observed in the control experiments with no LPC applied. Using pit assay, we verified

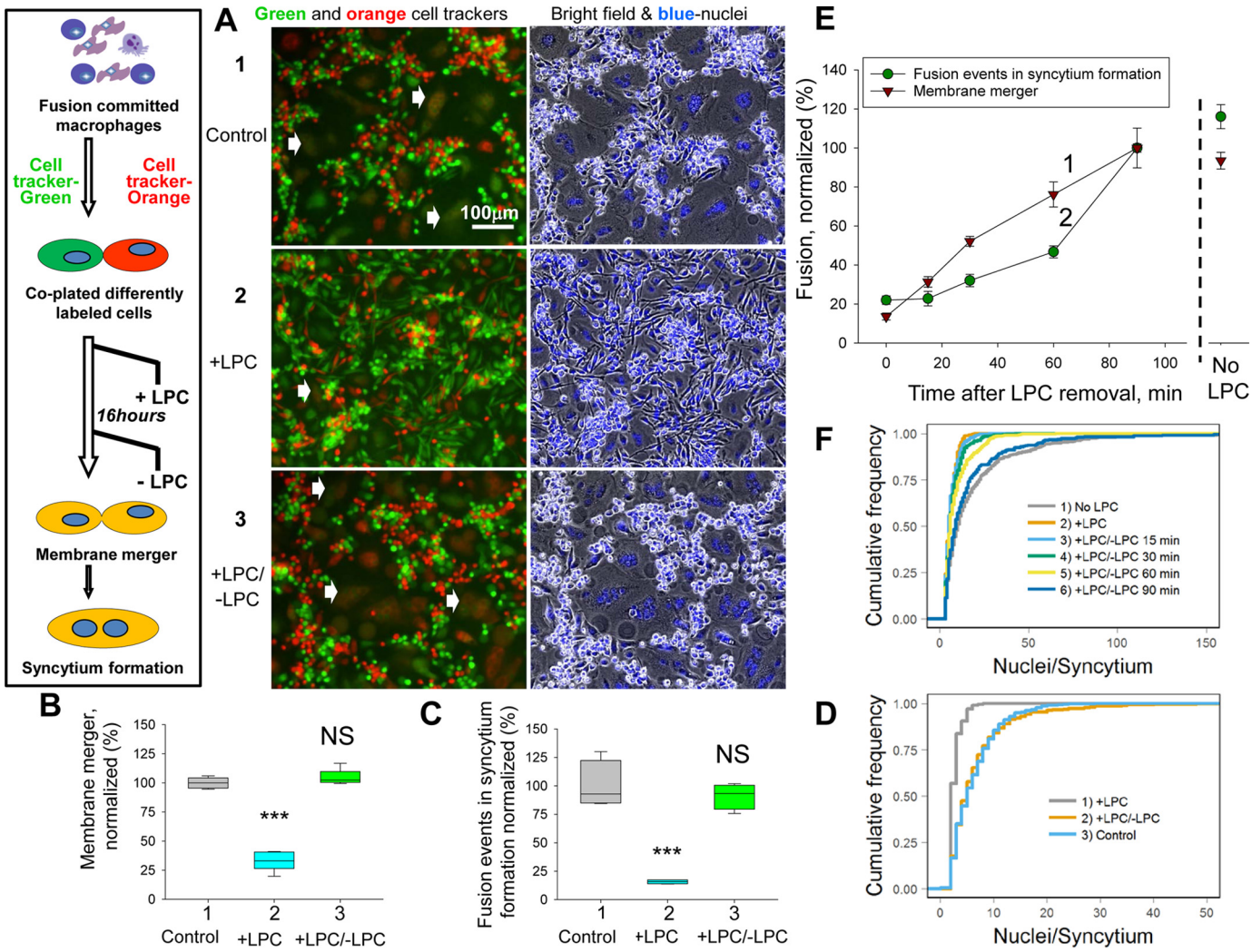

Figure 1. Synchronization of fusion between osteoclast precursors using hemifusion-inhibiting lipid LPC. *A,* in our standard experimental design, we synchronized OCP fusion by placing the differentiating OCPs into LPC-containing medium for a 16-h time interval and then washed LPC out to allow fusion. 90 min after LPC removal (= 89.5 h post-RANKL application), we took images of the cells for off-line analysis. Fluorescence (*left*) and bright field with stained nuclei (*right*) microscopy images illustrate synchronized fusion of HM-derived OCPs pre-labeled with either green or orange cell tracker. *1,* Control, control experiment in which fusion developed without LPC interruption. *2, +LPC,* LPC was applied but was not removed. *3, +LPC/−LPC,* LPC was applied and washed out. *Arrows* mark some of the double-labeled syncytia. The *left panel* illustrates experimental design. *B–D,* experiments on fusion between HM-derived OCPs such as the one in *A* were quantified to evaluate membrane merger (*B*), number of cell fusion events (*C*), and CDF characterizing the sizes of the syncytia (*D*). *1,* control experiments (no LPC applied); *2,* LPC applied and not removed; *3,* LPC applied and removed. *E* and *F,* fusion between RAW cell-derived OCPs was assayed at different times after LPC removal as membrane merger (*E, curve 1*) and as the total number of cell fusion events in syncytium formation (*E, curve 2*). *No LPC,* fusion extents and syncytium size distribution observed at 89.5 h post-RANKL application for the cells not treated with LPC. *F,* CDF analysis of the sizes of the syncytia. *B, C,* and *E,* membrane merger extents and numbers of cell fusion events generating syncytia were normalized to those observed in +LPC/−LPC experiments 90 min after LPC removal. Data from 10 random imaging fields for each condition in a single representative experiment out of three repeats are presented as curves (*E*) and box plots (*B* and *C*) with *center lines* showing the medians; box limits indicate the 25th and 75th percentiles and whiskers above and below the *box* indicate the 90th and 10th percentiles. Levels of significance relative to the data in control (*box plots 1*) are shown as not significant (*NS*, $p > 0.05$) and ***, $p < 0.001$.

that human osteoclasts formed after fusion synchronization had the same bone resorption activity as osteoclasts formed without LPC application (Fig. S1).

In the experiments presented in Fig. 1, *E* and *F*, we used the fusion synchronization approach in osteoclast formation by RAW cells to compare the time course of membrane merger, and syncytium formation, after LPC removal. Earlier fusion stages detected with the membrane merger assay developed faster than syncytium formation stages (Fig. 1*E*, *curve 1 versus curve 2*). Analysis of the number of completed fusion events (Fig. 1*E*, *curve 2*) and the CDF analysis (Fig. 1*F*) showed the lack of detectable syncytium formation in the first 15 min after LPC removal. This lag period most likely represents the minimal time from initiation to completion of a cell fusion event.

Fusion suppression with LPC has allowed us to uncouple the cell fusion stage of formation of human and murine multinucleated osteoclasts, operationally defined here as processes starting from LPC removal and ending with membrane merger, from the pre-fusion differentiation processes. Note that fusion recovery after LPC removal developed in the absence of RANKL and antibodies to RANK had no effect on the synchronized fusion of HM-derived OCPs (Fig. 2, *A* and *B*), indicating that whereas RANKL signaling triggers osteoclastogenic differ-

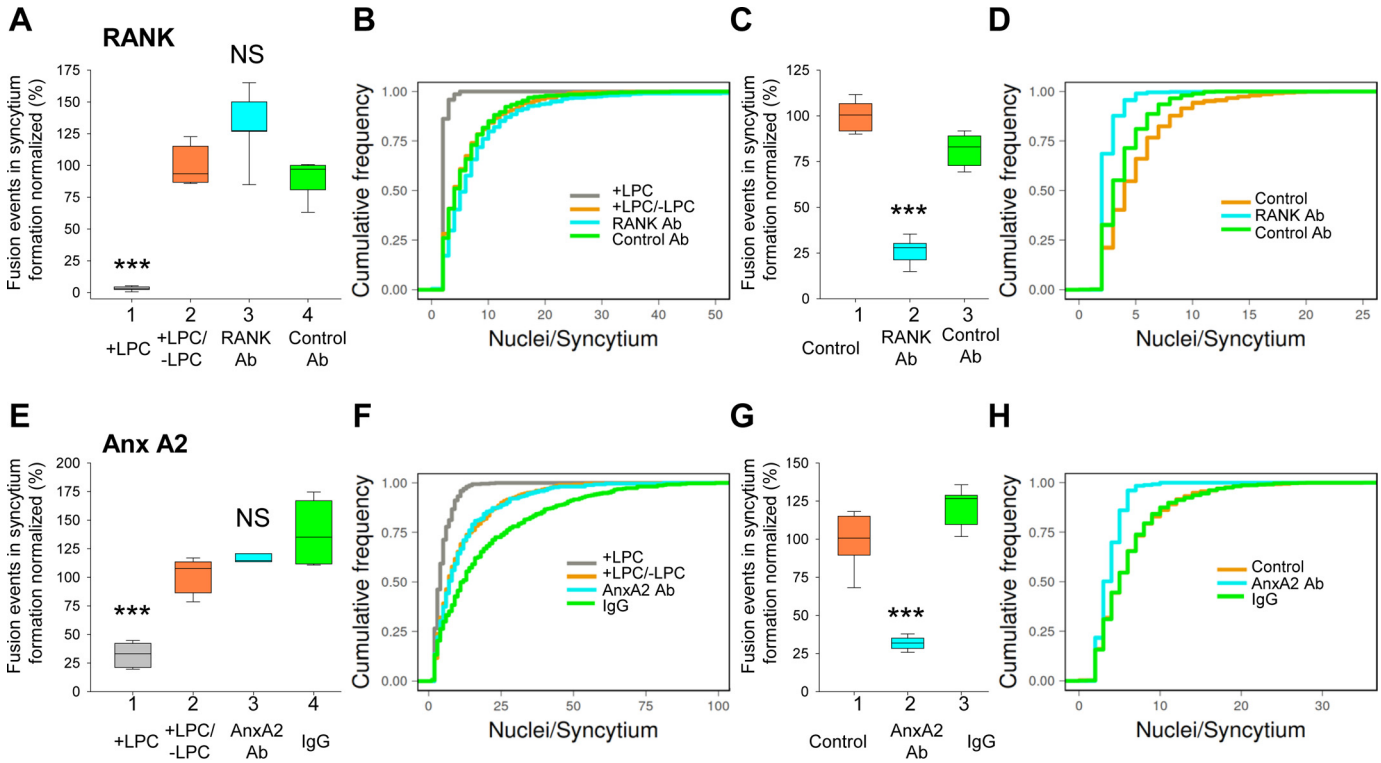

Figure 2. Antibodies to RANK (*A–D*) and Anx A2 (*E–H*) proteins functioning in early stages of osteoclastogenesis do not inhibit synchronized fusion between human osteoclast precursors. *A* and *B*, RANK antibody (20 μg/ml) added at the time of LPC removal (*i.e.* at 88 h post-RANKL application) had no effect on the synchronized osteoclast fusion. *1*, LPC was not removed; *2–4*, LPC was applied and removed with no antibodies applied (*2*) or with either RANK antibody (*3*) or negative control antibody (fish G-7 antibody (*4*)) applied. *C* and *D*, RANK antibody (2 μg/ml) added at 72 h post-RANKL application inhibits formation of multinucleated osteoclasts. *1*, control (no antibodies applied); *2*, RANK antibody; *3*, negative control antibody (fish G-7 antibody). *E* and *F*, Anx A2 antibody (30 μg/ml) added at the time of LPC removal (*i.e.* at 88 h post-RANKL application) had no effect on the synchronized osteoclast fusion. *1*, LPC was not removed; *2*, no antibodies applied; *3*, Anx A2 antibody; *4*, non-specific IgG. *G* and *H*, Anx A2 antibody (10 μg/ml) added at 72 h post-RANKL application inhibits formation of multinucleated osteoclasts. *1*, control (no antibodies applied); *2*, Anx A2 antibody; *3*, non-specific IgG. Fusion efficiency was characterized as the total number of cell fusion events in syncytium formation (*A*, *C*, *E*, and *G*) and as the CDF of syncytium sizes (*B*, *D*, *F*, and *H*). *A*, *C*, *E*, and *G*, data from 10 random imaging fields for each condition in a single representative experiment out of three repeats are presented as *box plots* with *center lines* showing the medians; box limits indicate the 25th and 75th percentiles and whiskers above and below the *box* indicate the 90th and 10th percentiles. Fusion extents were normalized to those observed in +LPC/−LPC experiments 90 min after LPC removal (*A* and *E*) or in the control (*C* and *G*, no antibodies applied). Levels of significance relative to the +LPC/−LPC data (*A* and *E*) or to the control (*C* and *G*) are shown as not significant (*NS*, $p > 0.05$) and ***, $p < 0.001$.

entiation leading to fusion, fusion itself does not depend on activity of the RANK. Antibodies to Anx A2, a protein that stimulates the proliferation and differentiation of osteoclast precursors at early stages of osteoclastogenesis (36, 37), also had no effect on the synchronized fusion of HM-derived OCPs (Fig. 2, *E* and *F*). As expected, application of even lower concentrations of the same RANK and Anx A2 antibodies at earlier times post-RANKL application strongly inhibited formation of multinucleated osteoclasts (Fig. 2, *Cx*, *D*, *G*, and *H*).

In summary, the fusion-synchronization approach allows us to characterize the effects of different treatments and reagents on 90 min of robust fusion rather than on several days of osteoclastogenic differentiation and thus to distinguish proteins involved in fusion from proteins involved only in pre-fusion differentiation such as RANK and Anx A2.

Fusion dependence on DC-STAMP and syncytin-1

Formation of multinucleated osteoclasts is completely abrogated in DC-STAMP-deficient cells (21). We used the fusion synchronization approach to examine whether DC-STAMP functions in the cell fusion stage of osteoclast formation. Application of DC-STAMP antibodies but not of the control IgG to RAW cells at the time of LPC removal lowered the number of completed cell fusion events, blocked formation of large syncytia, and inhibited membrane merger (Fig. 3, *A–D*), suggesting that this protein is directly involved in fusion. DC-STAMP antibodies also inhibited synchronized fusion of HM-derived OCPs (Fig. 3*E*).

Osteoclastogenic differentiation and formation of HM-derived multinucleated osteoclasts have been reported to involve Syn-1 (32). In agreement with earlier reports, we found that HM-derived OCPs express Syn-1 (Fig. 4*A*). To focus on the fusion stage of osteoclastogenesis, we accumulated ready-to-fuse HM-derived OCPs, using LPC block, and applied Syn-1-targeting reagents at the time of LPC removal. Antibodies to Syn-1, but not the control antibodies, lowered the number of completed fusion events and blocked formation of large syncytia (Fig. 4, *B* and *C*). To further examine the role of Syn-1, we used a peptide inhibitor of Syn-1-mediated fusion (32, 38). Fusogenic activity of the transmembrane subunit of Syn-1 depends on the association between N- and C-terminal heptad repeat regions of the protein in a 6-helix bundle fusion-active core. A peptide derived from the C-terminal heptad repeat inhibits this association and thus inhibits Syn-1-mediated fusion. We found that application of Syn-1 peptide, but not of its scrambled version, at the time of LPC removal decreases the

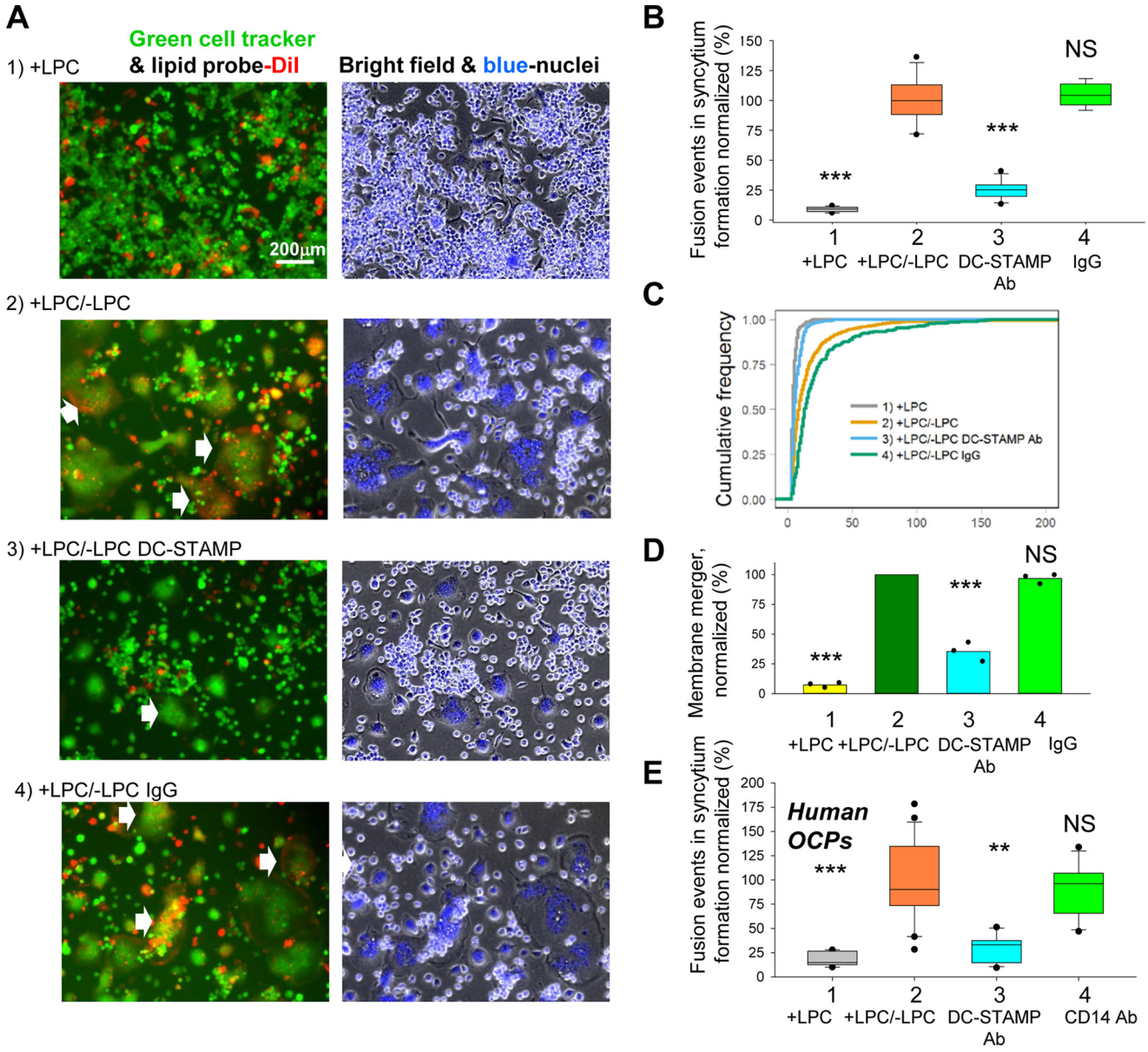

Figure 3. Synchronized fusion depends on DC-STAMP. *A,* fluorescence (*left*) and bright field with stained nuclei (*right*) microscopy images of the synchronized fusion between RAW cell-derived OCPs pre-labeled with either green cell tracker or DiI. At the time of LPC removal, we applied DC-STAMP antibody (*3*), non-specific IgG (*4*), or neither (*2*). *1,* LPC was not removed. *Arrows* mark some of the double-labeled syncytia. *B–D,* effects of DC-STAMP antibodies on the synchronized fusion between RAW cell OCPs in the experiments such as the one shown in *A* were quantified to evaluate the number of cell fusion events (*B*), the CDF characterizing the sizes of the syncytia (*C*), and membrane merger (*D*). *1,* LPC was not removed; *2,* LPC was applied and removed; *3* and *4,* DC-STAMP antibody (*3*) or non-specific IgG (*4*) were applied at the time of LPC removal. *E,* DC-STAMP antibodies lower the number of synchronized cell fusion events between HM-derived OCPs. *1,* LPC was not removed; *2,* LPC was applied and removed; *3* and *4,* DC-STAMP antibody (*3*) or antibody to macrophage marker CD14 used as a negative control (*4*) was applied at the time of LPC removal. *B, D,* and *E,* membrane merger extents and the numbers of cell fusion events were normalized to those observed in +LPC/−LPC experiments (*2*). *B* and *E,* data from 10 random imaging fields for each condition in a single representative experiment out of three repeats are presented as *box plots* with *center lines* showing the medians; box limits indicate the 25th and 75th percentiles, and whiskers above and below the *box* indicate the 90th and 10th percentiles. *Dots* show outlying points. *D,* data for three independent experiments for each condition shown as means (*bars*) and individual points. Levels of significance relative to the +LPC/−LPC data are shown as not significant (*NS*, $p > 0.05$) and ** and ***, for $p < 0.01$ and $p < 0.001$.

number of completed cell fusion events, suppresses formation of large syncytia, and inhibits membrane merger in synchronized fusion between HM-derived OCPs (Fig. 4, *D–G*). These findings suggested the dependence of the cell fusion stage of osteoclastogenesis on Syn-1. Moreover, since Syn-1 molecules involved in fusion were susceptible to the Syn-1 peptide inhibition, we conclude that these molecules are (i) expressed at the surface of the cells and (ii) undergo fusogenic restructuring into 6-helix bundles blocked by the peptide.

In summary, our findings show that DC-STAMP and Syn-1, both known to play an important role in formation of multinucleated osteoclasts and suggested to function at the fusion stage of osteoclastogenesis (21, 32), are indeed involved in osteoclast fusion.

Fusion depends on phosphatidylserine externalization

Because macrophage fusion in the generation of the giant cells of inflammation is associated with PS exposure at the cell

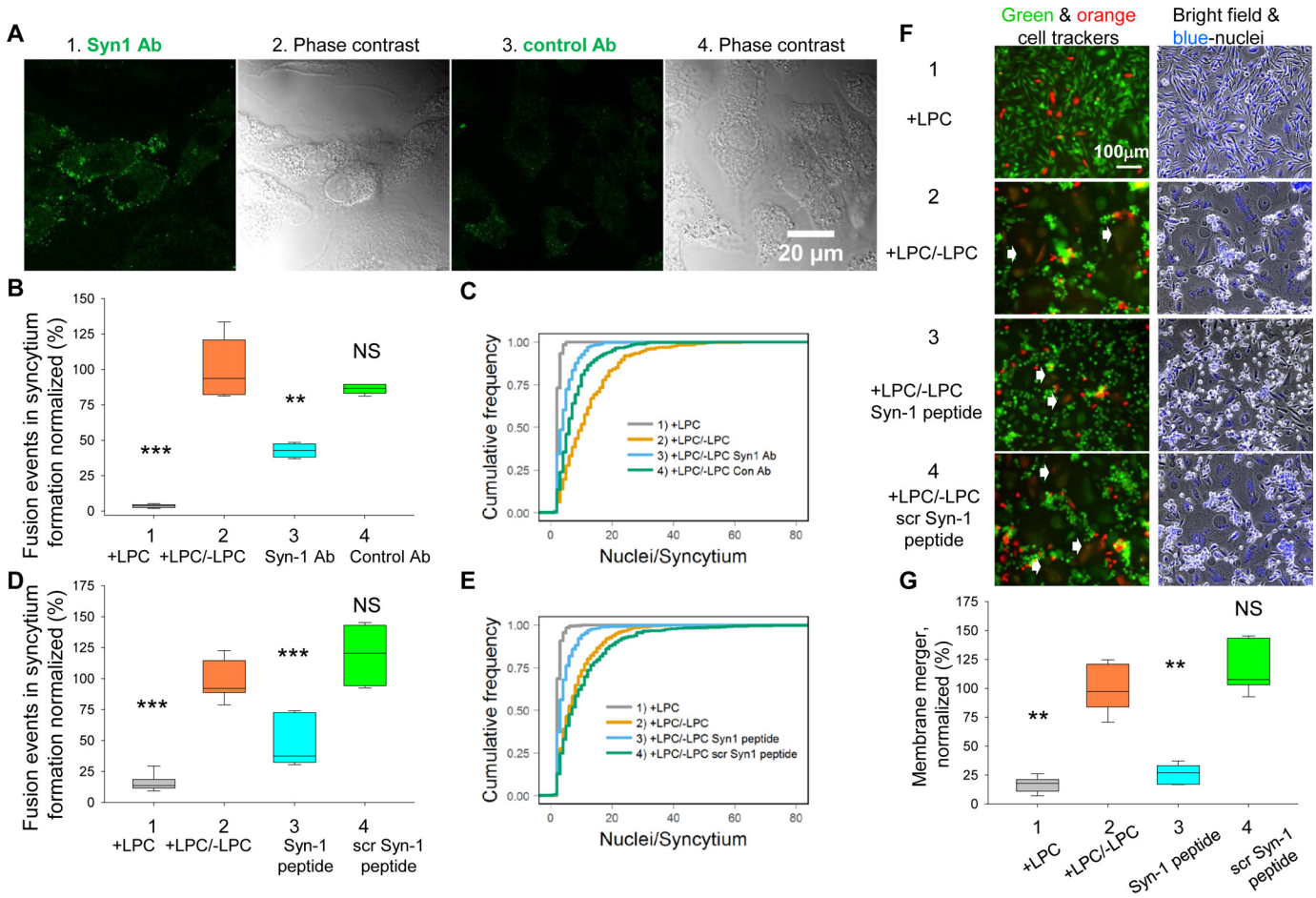

Figure 4. Synchronized fusion of human osteoclast precursors depends on Syn-1. *A,* immunofluorescence microscopy confirms Syn-1 presence on the surface of fusion-committed HM-derived OCPs. Fluorescence (*1* and *3*) and phase contrast (*2* and *4*) images of the cells were taken at 89.5 h post-RANKL application. The cells were stained with either Syn-1 antibody (*1* and *2*) or myogenin antibody used as a negative control (*3* and *4*); followed with Alexa Fluor 488-tagged secondary antibodies (*green*). *B–E,* Syn-1 antibody (*B* and *C*) and Syn-1 peptide (*D* and *E*) inhibit synchronized fusion between HM-derived OCPs. LPC was removed in the presence of Syn-1 antibody (*B3* and *C, curve 3*), or Syn-1 peptide (*D3* and *E, curve 3*) or control (myogenin) antibody (*B4* and *C, curve 4*), or scrambled Syn-1 peptide (*D4* and *E, curve 4*) (*2*). *B* and *D* and *curves 2* in *C* and *E,* neither antibodies nor peptides applied (*1*). *B* and *D* and *curves 1* in *C* and *E,* LPC was not removed. Fusion efficiency was characterized as the total number of cell fusion events in syncytium formation (*B* and *D*) and as the CDF of syncytium sizes (*C* and *E*). *F* and *G,* fluorescence (*left*) and bright field with stained nuclei (*right*) microscopy images (*F*) and quantification (*G*) show Syn-1 peptide inhibition of the membrane merger stage in fusion between HM-derived OCPs pre-labeled with either green or orange cell tracker. At the time of LPC removal, we applied Syn-1 peptide (*3*) or a scrambled peptide (*4*) or neither (*2*). *1,* LPC was not removed. *Arrows* mark some of the double-labeled syncytia. *B, D,* and *G,* total numbers of cell fusion events and membrane merger extents were normalized to those observed in +LPC/−LPC experiments (*box plots 2*). *B, D,* and *G,* data from 10 random imaging fields for each condition in a single representative experiment out of three repeats are presented as *box plots* with *center lines* showing the medians; box limits indicate the 25th and 75th percentiles, and whiskers above and below the *box* indicate the 90th and 10th percentiles. Levels of significance relative to the +LPC/−LPC data are shown as not significant (*NS*, $p > 0.05$) and ***, for $p < 0.001$.

surface (11), we examined the role of PS externalization in fusion of monocyte/macrophage lineage OCPs. First, to evaluate cell-surface levels of PS, we stained the HM-derived OCPs with the PS-specific probe, fluorescently-labeled Anx A5, and examined cells using fluorescence microscopy. Anx A5 labeling of HM-derived OCPs was significantly higher than that of proliferating HM-derived macrophages (Fig. 5, *A* and *B*), suggesting that development of fusion competence in OCPs correlates with elevated levels of cell-surface PS. Importantly, PS exposure on the HM-derived OCPs with cell-surface PS correlated neither with activation of caspases 3 or 7 nor with cell nuclei labeling by the membrane-impermeable probe TO-PRO-3, both characteristic features of apoptotic cells (Fig. S2).

Non-apoptotic externalization of PS involves proteins of the TMEM16 family containing Ca^{2+}-activated lipid scramblases and chloride channels (39). An inhibitor of these TMEM16 channels and of PS externalization (40), CaCCinh-A01 (referred henceforth as A01), suppressed PS exposure in HM-derived OCPs (Fig. 5*B*) and lowered the numbers of completed fusion events and large syncytia in the synchronized fusion of HM-derived OCPs (Fig. 5, *C* and *D*). A01 also inhibited fusion between RAW cell-derived OCPs (Fig. S3). These findings suggested that PS externalization is important for OCP fusion. This conclusion was further strengthened by the finding that blocking cell-surface PS with the PS-binding protein lactadherin (41) inhibited synchronized fusion (Fig. 5, *E* and *F*).

Taking into account the dependence of PS externalization on the intracellular calcium (39) and the involvement of DC-STAMP in the regulation of calcium signaling network (22), we tested whether OCP fusion inhibition by DC-STAMP antibodies (Fig. 3*E*) correlates with any changes in the amounts of the cell-surface PS. Indeed, as shown in Fig. 5, *G* and *H*, application

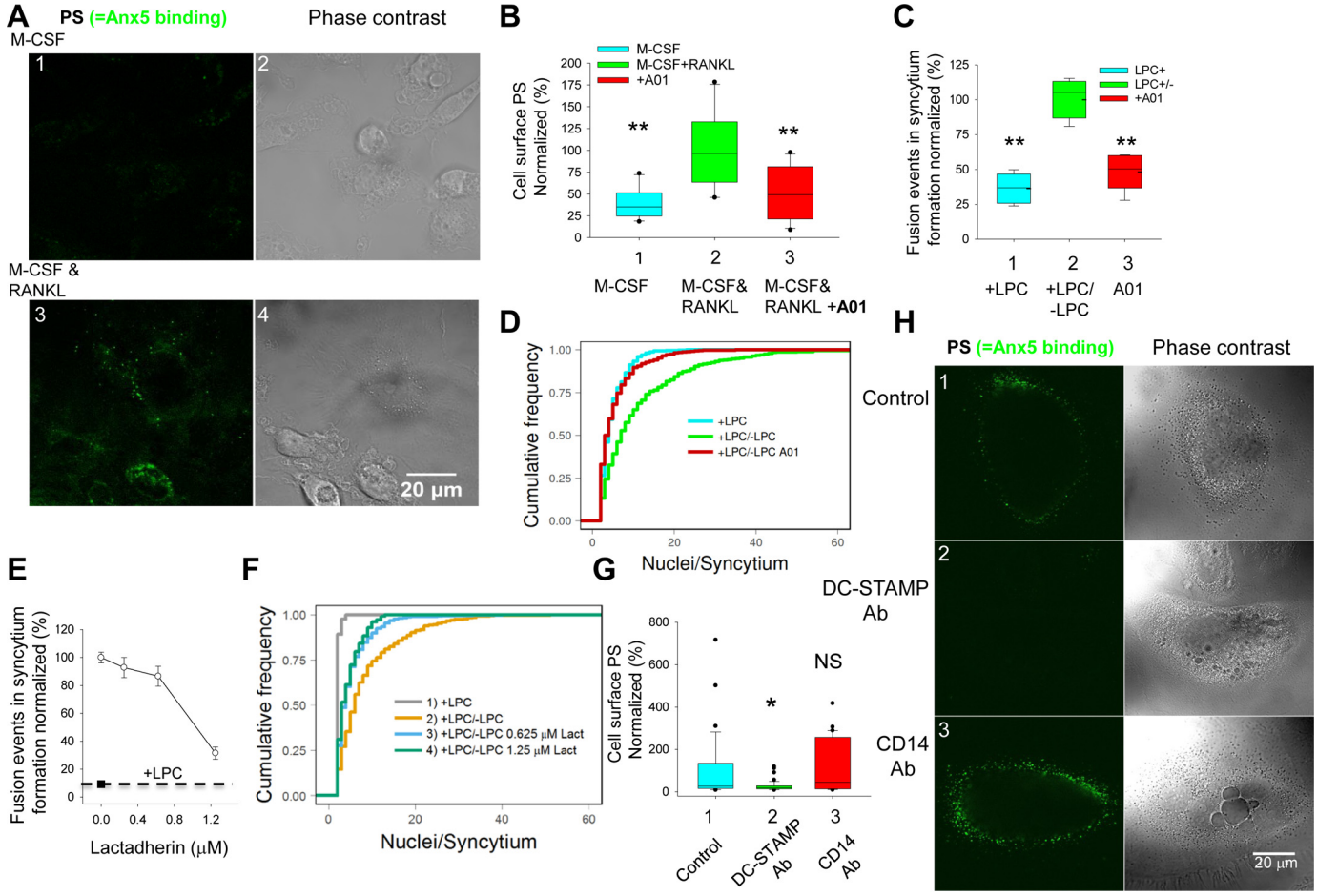

Figure 5. Synchronized fusion depends on PS at the surface of fusion-committed HM-derived osteoclast precursors. *A* and *B*, PS at the surface of non-permeabilized fusion-committed OCPs and HM-derived macrophages detected as Alexa Fluor 488-tagged Anx A5 (*green*) labeling. *A*, fluorescence (*1* and *3*) and phase contrast (*2* and *4*) images of the OCPs were taken at 89.5 h post-RANKL application or, for macrophages, at 233.5 h post M-CSF application. *B*, PS amounts on the surface of the macrophages (*1*) and on the fusion-committed OCPs not-treated (*2*) or treated with A01 (*3*) were normalized to (*2*). PS amounts were quantified for >150 cells for each condition in a single representative experiment out of three repeats. *C–F*, lowering the amounts of accessible cell-surface PS with A01 (*C* and *D*) or with PS-binding protein lactadherin (*E* and *F*) applied at the time of LPC removal inhibited synchronized fusion of HM-derived OCPs (*1*). *C* (*1*) and *dashed line* in *E*, LPC was not removed. Fusion efficiencies in seven random imaging fields for each condition in a single representative experiment out of three repeats were characterized as the total number of cell fusion events in syncytium formation normalized to those observed in +LPC/−LPC experiments with neither A01 nor lactadherin applied (*C* and *E*). *D* and *F*, distributions of the sizes of syncytia in the experiments shown in *C* and *E* are presented as CDF. *G*, application of DC-STAMP antibodies lower the amounts of cell-surface PS. The amounts of the cell-surface PS on the OCPs treated with antibodies (20 μg/ml) to DC-STAMP (*2*) or to CD14 (*3*), used as a negative control, were normalized to the PS amounts for the untreated OCPs (*1*). PS amounts were quantified for ≥50 cells for each condition in a single representative experiment out of three repeats and presented as *box plots*. *H*, fluorescence microscopy images illustrating a decrease in cell-surface PS caused by application of DC-STAMP antibody. *Left*, Alexa Fluor 488-tagged Anx A5 (*green*) labeling. *Right*, phase contrast. Images of the OCPs treated with antibodies to DC-STAMP (*2*) or CD14 (*3*) or with neither (*1*) were taken 2 h after LPC removal. In the *box plots* in *B*, *C*, and *G*, *center* and *dashed lines* show the medians and means; box limits indicate the 25th and 75th percentiles, whiskers above and below the *box* indicate the 90th and 10th percentiles, and *dots* show outlying points. Levels of significance relative to the M-CSF and RANKL experiments (*B*), or to +LPC/−LPC experiments (*C*), or to control (no antibody added) (*G*) are shown as not significant (*NS*, for $p > 0.05$) and *, $p < 0.05$; **, $p < 0.01$.

of a fusion-inhibiting concentration of the antibodies lowered Anx A5 labeling of HM-derived OCPs.

To summarize, the presence of PS at the surface of fusion-committed OCP cells, the dependence of cell-surface PS on DC-STAMP activity, and fusion inhibition by reagents that either suppressed this exposure or blocked accessible PS, indicated that PS exposure plays an important role in the OCP fusion. These data suggested that fusion should also depend on some PS-binding proteins such as Anxs.

Annexins and S100A4 in osteoclast fusion

We found osteoclastogenic differentiation of HMs upon RANKL application to be associated with a strong increase in the amount of Anx A5 present at the cell surface (Fig. 6, *A* and *B*). Because extracellular Anxs A1 and A5 play an important role in the fusion stage of myogenesis (7), we tested whether synchronized fusion of HM-derived OCPs also depends on these two Anxs. Anx A5-targeting reagents (Anx A5 antibody and a synthetic peptide derived from the N-terminal domain of Anx A5 (7)) lowered the number of completed cell fusion events and inhibited formation of large syncytia (Fig. 6, *C–F*). However, Anx A1-targeting reagents had no effect on fusion of HM-derived OCPs, suggesting that Anx A1 is not involved in the fusion stage of formation of human osteoclasts. Finding that Anx A5 peptide but not the control scrambled peptide inhibited membrane merger (Fig. 6, *G* and *H*) confirmed that Anx A5 functions at the early rather than late stages of human osteoclast fusion.

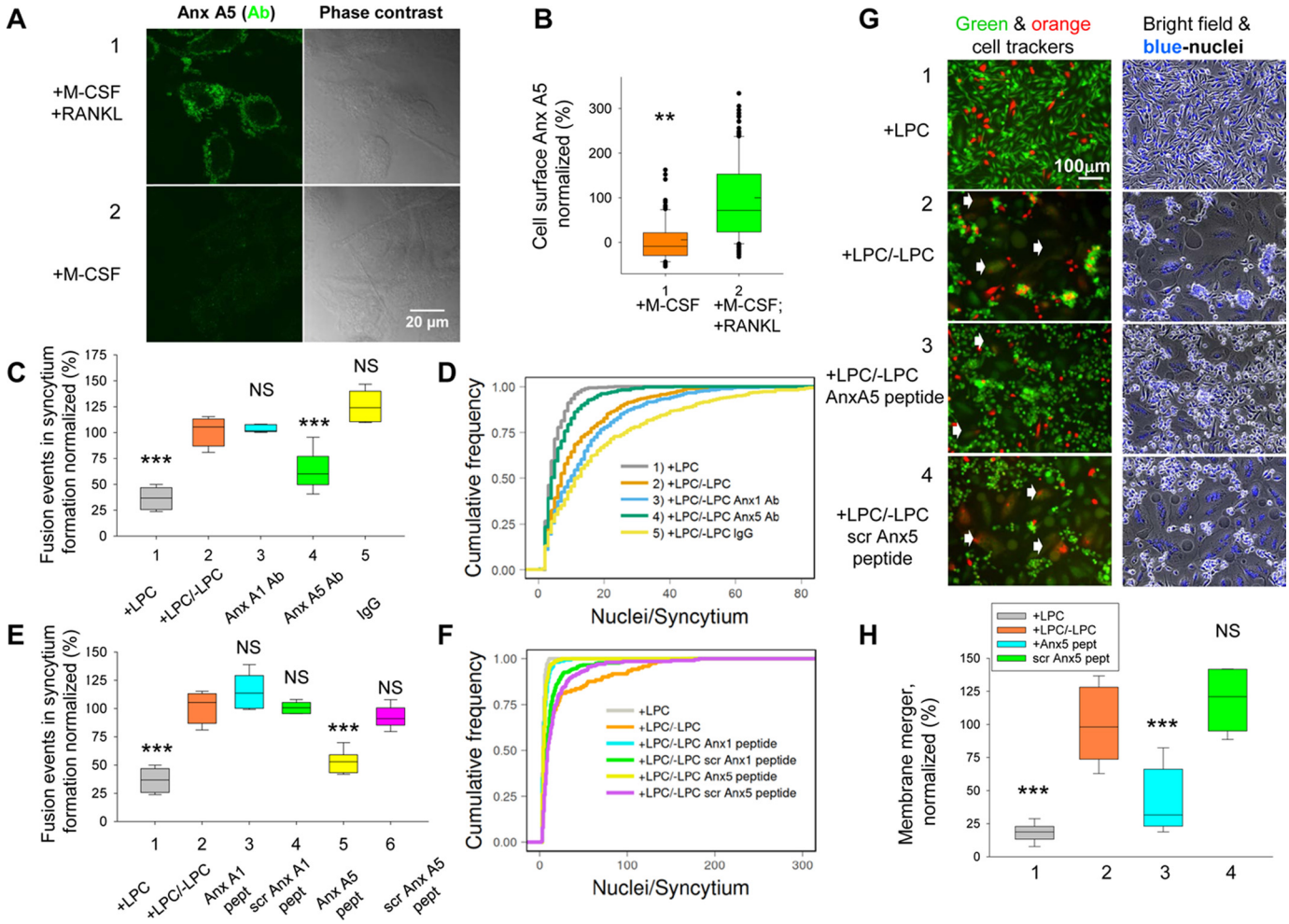

Figure 6. Synchronized fusion of human osteoclast precursors depends on Anx A5. *A* and *B,* HM-derived OCPs (*1*) but not HM-derived macrophages (*2*) display Anx A5 at the surface of non-permeabilized cells, as evidenced by cell-surface labeling with Anx A5 antibody (*green*). Fluorescence (*left*) and phase contrast (*right*) images of the HM-derived OCPs (*1*) and HM-derived macrophages (*2*) were taken at 89.5 h post-RANKL application (= 233.5 h post M-CSF application) and at 233.5 h post M-CSF application, respectively. The cells were stained with Anx A5 antibody followed by Alexa Fluor 488-tagged secondary antibodies (*green*). *B,* amounts of Anx A5 at the cell surface (quantified from Anx A5 antibody binding) were higher for non-permeabilized HM-derived OCPs (*2,* "+*M-CSF*+*RANKL*") than those for the HM-derived macrophages (*1,* "+*M-CSF*"). Anx A5 amounts were quantified for ≥150 cells for each condition in a single representative experiment out of three repeats. *C–F,* Anx A5-targeting reagents applied at the time of LPC removal inhibited synchronized fusion of HM-derived OCPs. Anx A5 antibody (*C* and *D*) and Anx A5 peptide (*E* and *F*) but neither Anx A1 antibody nor non-specific IgG (*C* and *D*) nor Anx A1 peptide nor scrambled Anx A1/A5 peptides (*E* and *F*) lowered the total number of fusions between HM-derived OCPs in syncytium formation (*C* and *E*) and decreased the sizes of the syncytia (*D* and *F*). *G,* fluorescence (*left*) and bright field with stained nuclei (*right*) microscopy images show that Anx A5 peptide but not its scrambled version inhibits the membrane merger stage of fusion between HM-derived OCPs pre-labeled with either green or orange cell tracker. At the time of LPC removal, we applied Anx A5 peptide (*3*) or a scrambled peptide (*4*) or neither (*2*). *1,* control experiment in which LPC was not removed. *Arrows* mark some of the double-labeled syncytia. *H,* quantification of membrane merger extents in the experiments like the one presented in *G*. *B, C, E,* and *H,* cell-surface Anx A5 labeling (*B*) and total numbers of cell fusion events in syncytium formation (*C* and *E*) and membrane merger extents (*H*) were normalized to those observed in M-CSF and RANKL experiments (*B*) and in +LPC/−LPC experiments (*C, E* and *H, box plots 2*). Data from 10 random imaging fields for each condition in a single representative experiment out of three repeats are presented as *box plots* with *center lines* showing the medians; box limits indicate the 25th and 75th percentiles. Whiskers above and below the *box* indicate the 90th and 10th percentiles, and *dots* show outlying points. Levels of significance relative to the +M-CSF + RANKL experiments (*B*) or to the +LPC/−LPC data (*C, E,* and *H*) are shown as not significant (*NS* $p > 0.05$) and **, $p < 0.01$, and ***, $p < 0.001$.

To test whether fusion between RAW cell-derived OCPs also involves extracellular Anxs, we accumulated ready-to-fuse OCPs in the presence of LPC and at the time of LPC removal added antibodies to Anxs A1 or A5 (Fig. 7, *A* and *B*). In contrast to control IgG, Anx A1 and A5 antibodies decreased the number of completed cell fusion events and the sizes of the syncytia. Application of the synthetic peptides derived from the N-terminal domain of these Anxs similarly inhibited synchronized fusion of RAW cell-derived OCPs (Fig. 7, *C* and *D*). Thus, fusion between murine OCPs derived from RAW cells depended on both Anx A5 and Anx A1, whereas fusion between HM-derived OCPs depended on extracellular Anx A5 but not Anx A1.

The importance of Anxs A1 and A5 in murine OCP fusion was confirmed in the experiments on osteoclast formation by murine BMC. We compared osteoclast formation from BMCs from mice deficient in either Anx A1 or A5 with that from BMCs isolated from WT mice (Fig. 7, *E–G*). Although we observed the appearance of multinucleated cells in the absence of either of these Anxs, the numbers of completed cell fusion events and the sizes of the multinucleated cells were strongly decreased *versus* those observed for BMCs from WT mice (Fig. 7, *E–G*). As expected for proteins involved in fusion rather than in the pre-fusion stages of osteoclastogenesis, neither Anx A1 nor Anx A5 deficiency had an effect on TRAP-staining intensity (Fig. 7, *E* and *F*).

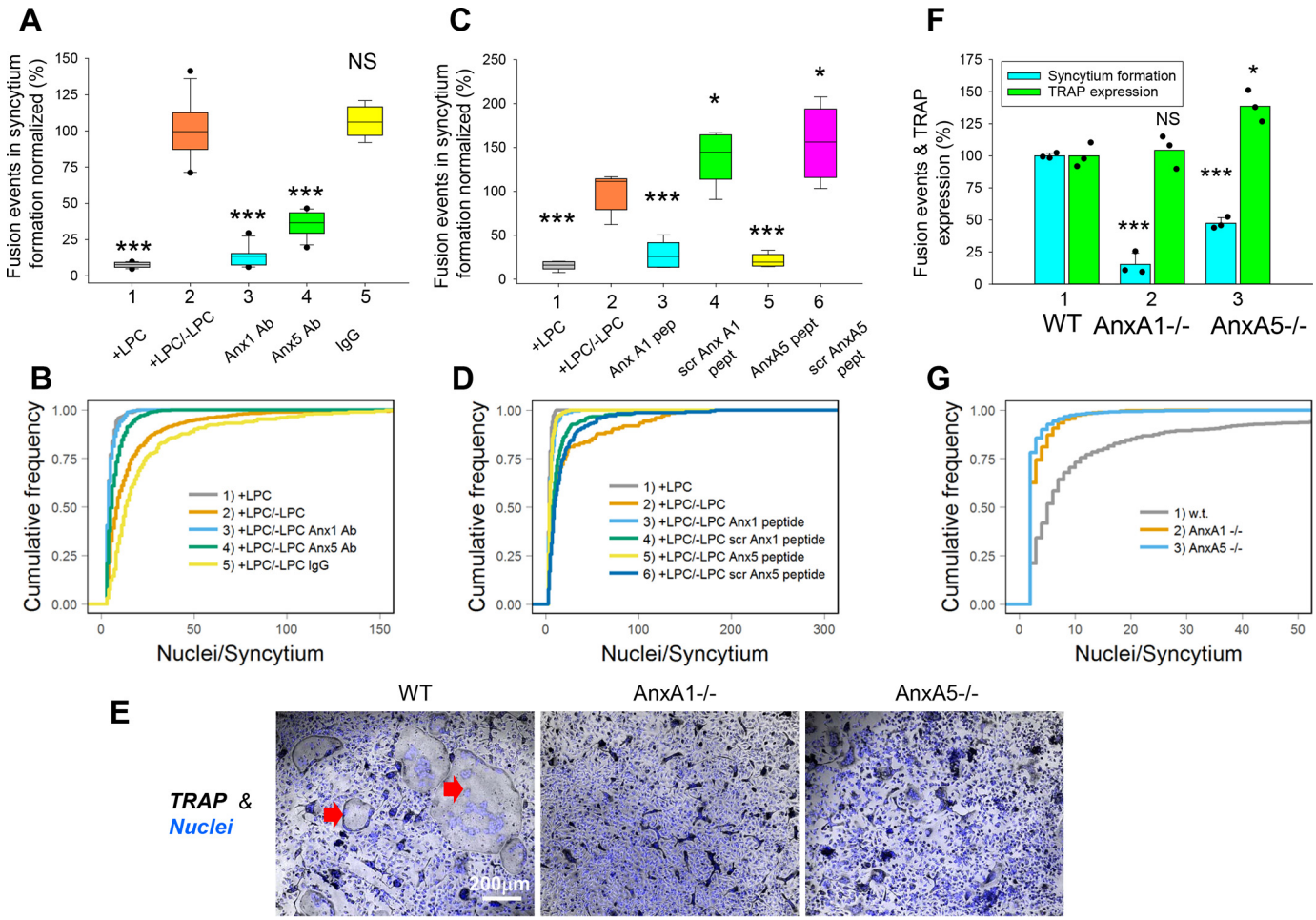

Figure 7. Fusion between murine osteoclast precursors depends on Anxs A1 and A5. *A–D,* reagents targeting either Anx A1 or AnxA5 applied at the time of LPC removal inhibited synchronized fusion of OCPs derived from RAW cells. Anxs A1 and A5 antibodies (*A* and *B*) and Anxs A1 and A5 peptides (*C* and *D*) but neither non-specific IgG (*A* and *B*) nor scrambled peptides (*C* and *D*) lowered the total number of cell fusion events in syncytium formation (*A* and *C*) and decreased the sizes of the syncytia (*B* and *D*). *A* and *C,* total numbers of cell fusion events in syncytium formation were normalized to those observed in +LPC/−LPC experiments 90 min after LPC removal (*2*). Data from 10 random imaging fields for each condition in a single representative experiment out of three repeats are presented as *box plots* with *center lines* showing the medians; box limits indicate the 25th and 75th percentiles. Whiskers above and below the *box* indicate the 90th and 10th percentiles, and *dots* show 95th and 5th percentiles. *E,* images of TRAP-stained osteoclasts generated from BMCs of WT mice or mice deficient in either Anx A1 or A5. Although all three images show similar total intensities of the TRAP staining, only WT BMC generated large multinucleated osteoclasts such as those marked by *red arrows*. *F,* numbers of cell fusion events and the total intensities of the TRAP staining for WT (*1*), Anx A1-deficient (*2*), and Anx A5-deficient BMCs were normalized to those for WT BMCs. Data are shown as individual points from independent experiments (each point corresponds to bone marrow cells from one of three mice per condition) and *bars* show means ± S.D. *G,* CDF for the osteoclast sizes for BMCs from WT, Anx A1-deficient, and Anx A5-deficient mice (*1, 2, 3,* respectively). *A, C,* and *F,* levels of significance relative to the +LPC/−LPC data (*A* and *C*) or to WT (*F*) are shown as not significant (*NS,* $p > 0.05$) and *, $p < 0.05$, and ***, $p < 0.001$.

The finding that the synthetic peptide derived from the N terminus of Anx A5 inhibits fusion between OCPs suggested that this region of the protein is important for Anx A5 contributions to fusion. N-terminal regions of Anxs, including Anx A1 and Anx A5, contribute to the stability of the structure of Anxs and their self-assembly and mediate interactions between Anxs and their partner proteins, including proteins of the S100 family of calcium-binding proteins (42). To test whether Anx A5 peptide inhibits interactions between Anx A5 and its partners, we focused on S100A4, which has been shown to regulate osteoclastogenesis in mice (26, 43). Indeed, we found this protein to be present at the surface of fusion-committed HM-derived OCP cells (Fig. 8*A*) and antibodies to S100A4 to inhibit synchronized fusion (Fig. 8*B*). Application of a fusion-inhibiting concentration of Anx A5 peptide but not its scrambled version lowered the total amounts of S100A4 at the surface of the cells (Fig. 8, *A* and *C*). In contrast, Anx A5 peptide had almost no effect on the Anx A5 presence on the surface of HM-derived osteoclasts (Fig. 8*C*), as expected taking into account that the N-terminal region of membrane-bound Anx A5 is not involved in the Anx A5 interactions with PS-containing membrane (44).

Using immunofluorescence microscopy, we verified that all four proteins that we found to be involved in the fusion stage of formation of human osteoclasts (DC-STAMP, Syn-1, Anx A5, and S100A4) are expressed at the surface of the fusion-committed OCPs (Fig. S4). Based on comparison between HMs treated with both M-CSF and RANKL and HMs treated with only M-CSF, osteoclastogenic differentiation did not change the amounts of Syn-1, but increased the amounts of Anx A5 (Fig. 6, *A* and *B*), DC-STAMP, and S100A4 (Fig. S4). Accumulation of ready-to-fuse OCPs in the presence of LPC did not significantly change amounts of DC-STAMP, Syn-1, and S100A4 and

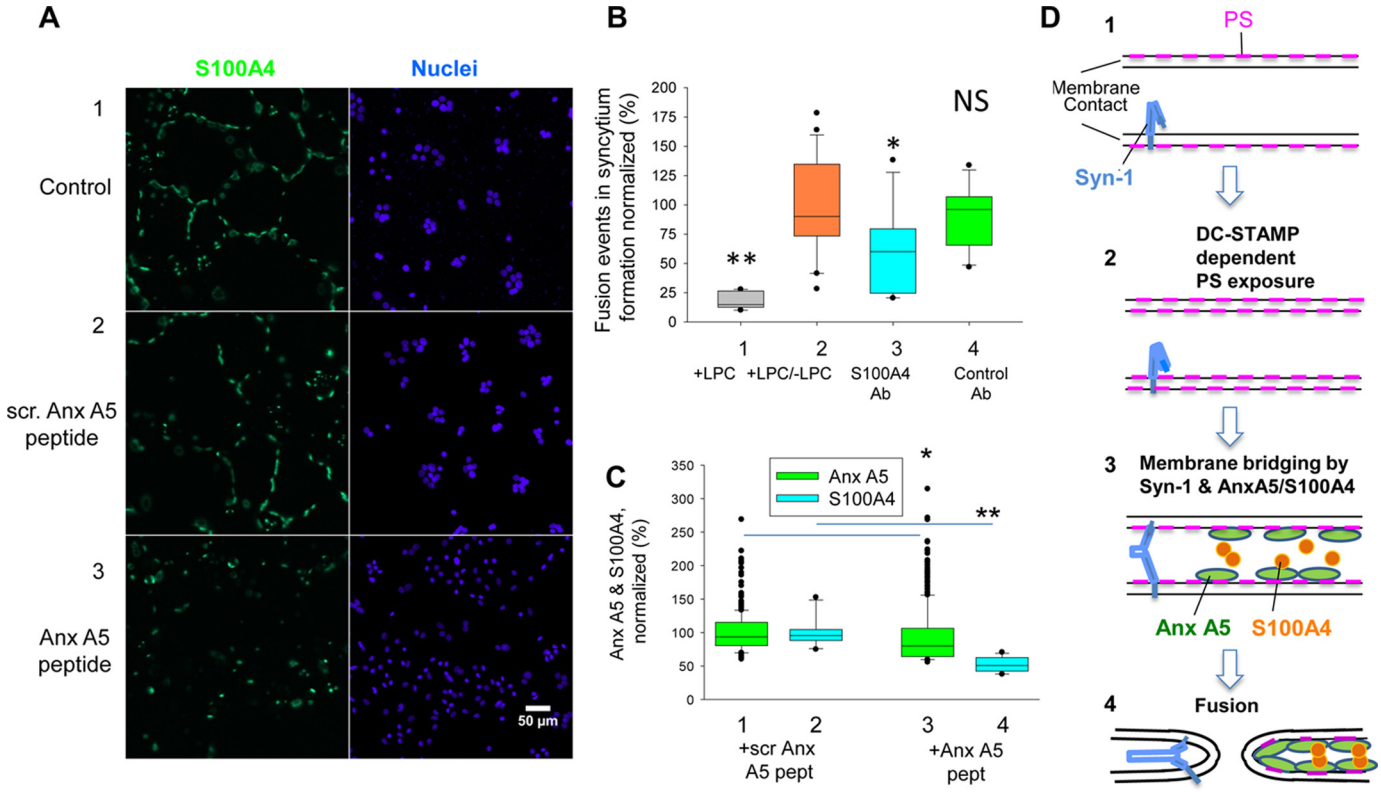

Figure 8. Fusion of osteoclast precursors depends on multiprotein machinery. *A,* fusion inhibitor Anx A5 peptide lowers amounts of S100A4 at the surface of HM-derived OCPs. Fluorescence microscopy images of the cells were taken at 89.5 h post-RANKL application. The non-permeabilized cells were stained to detect S100A4 (*green*). The cells were treated with scrambled Anx A5 peptide (*2*) or with Anx A5 peptide (*3*) or with neither of these peptides (*1*) for 90 min prior to taking the images. *B,* S100A4 antibody inhibits synchronized fusion between HM-derived OCPs. LPC was removed in the presence of S100A4 antibody (*3*), or CD14 antibody that was used as a negative control (*4*), or neither (*2*). *1*, −LPC was not removed. The numbers of cell fusion events were normalized to those observed in +LPC/−LPC experiments (*box plot 2*). Data from 10 random imaging fields for each condition in a single representative experiment out of two repeats are shown. *C,* Anx A5 and S100A4 amounts at the surface of non-permeabilized HM-derived OCPs were quantified from cell labeling with antibodies at 89.5 h post-RANKL application. Anx A5 peptide (*3* and *4*) had only a small effect on the cell-surface concentration of Anx A5 (*3*) but lowered the amounts of the cell-surface S100A4 (*4*). Scrambled Anx A5 peptide had no effect on either Anx A5 (*1*) or S100A4 (*2*) amounts at the surface of the cells. The amounts of the cell-surface Anx A5 and S100A4 were normalized to those at the cells not treated with the peptides. $n \geq 80$ cells for each condition in a representative experiment out of three repeats. Data in *B* and *C* are presented as *box plots* with *center lines* showing the medians. Box limits indicate the 25th and 75th percentiles. Whiskers above and below the *box* indicate the 90th and 10th percentiles, and *dots* show outlying points. Levels of significance relative to the +LPC/−LPC data (*B*) or to the control with scrambled Anx A5 peptide (*C*) are shown as not significant (*NS*, $p > 0.05$) and * and ** for $p < 0.05$ and $p < 0.01$, respectively. *D,* hypothetical mechanism in which downstream of DC-STAMP-dependent PS externalization Syn-1, Anx A5, and S100A4 collaborate in pulling the membranes together and initiating fusion.

slightly decreased amounts of Anx A5 (Fig. S4, *A–D*). Immunofluorescence microscopy experiments presented in Figs. S5 and S6 suggested that, whereas Anx A5, Syn-1, and S100A4 are not confined to cell–cell contacts, these proteins tend to be enriched and co-localized there. Although these findings are consistent with the results of our functional experiments suggesting the involvement of DC-STAMP, Syn-1, Anx A5, and S100A4 in fusion, the localization of these proteins at the time and place of fusion still awaits detailed characterization.

In summary, our findings suggest that osteoclast fusion depends on the ability of extracellular Anxs to form a protein scaffold that links the PS-presenting cell surface with S100A4 and, possibly, other protein partners of Anxs.

Discussion

Bone remodeling relies on a balance between bone formation by osteoblasts and bone resorption by osteoclasts. Osteoclast formation is a tightly regulated complex process that takes days and depends on many proteins. Synchronization of fusion between OCPs with the reversible inhibitor LPC has allowed us to uncouple the cell fusion stage of formation of human and murine multinucleated osteoclasts from most of the pre-fusion differentiation processes. We also uncoupled fusion from the post-fusion processes that complete unification of two cells by expanding the nascent membrane connections. We found synchronized fusion of human OCPs to depend on cell-surface PS, DC-STAMP, Syn-1, Anx A5, and S100A4. The dependence of OCP fusion on PS externalization, DC-STAMP, and Anxs (in this case both Anx A5 and Anx A1), was also observed for murine cells. As expected, synchronized fusion did not involve RANK and Anx A2, proteins reported to contribute at the early stages of osteoclastogenesis.

LPC-synchronized OCP fusion that developed in 60–90 min was slower than both LPC-synchronized myoblast fusion (20–30 min (7)) and cell–cell fusion mediated by many viral fusogens (within seconds or a few minutes (45)). It is possible that osteoclasts proceed along the fusion pathway as slowly as cells in fusion mediated by Ebola virus fusogen that takes several hours (46). Alternatively, the apparent slowness of the osteoclast fusion reflects the lack of stable contacts between mobile

OCPs. In this scenario, although transient contacts between fusion-committed cells in the presence of LPC do not yield fusion, after LPC removal, the new contacts between migrating cells lead to fusion.

PS exposure is a hallmark of several cell–cell fusion processes (11–13) but has never been reported for fusion of OCPs. Our finding that at the time of fusion OCPs display PS at their surface, and this PS exposure is required for fusion, raises questions on mechanisms that promote PS exposure in ready-to-fuse OCPs and on mechanisms by which cell-surface PS is involved in fusion. PS externalization depends on a sustained increase in intracellular calcium that promotes PS redistribution from the inner leaflet to the outer leaflet of the plasma membrane by scramblase activity (39). Formation of osteoclasts involves calcium signaling (47), and because this signaling is regulated by the immunoreceptor tyrosine-based inhibitory motif domain of DC-STAMP (22), we suggest that the role of this protein in the cell fusion stage of osteoclastogenesis is related to the calcium dependence of the PS exposure. Finding that DC-STAMP antibody inhibits PS exposure on fusion-committed OCPs substantiates the hypothesis that DC-STAMP is involved in the PS signaling processes that deliver this lipid to the surface of the cells and retain it there. The newly identified link between DC-STAMP activity and PS exposure can be also important in dendritic cells, where PS exposure has been suggested to regulate maturation of dendritic cells (48).

Functional importance of PS in the synchronized fusion suggests the involvement of PS-binding proteins. Indeed, we show that cell-surface PS engages extracellular Anxs, including Anxs A1 and A5. Anx A1 has been suggested as an osteoclastic protein, on the basis of its up-regulation in murine cells undergoing osteoclastogenic differentiation (49). To the best of our knowledge, Anx A5 has never been associated with osteoclast formation. Anxs have many interacting partners including S100A4, a protein reported to promote osteoclastogenesis (26, 43) and found here to be displaced by fusion-inhibiting Anx A5 peptide (Fig. 8, *A* and *B*).

Syn-1 has already been shown to function in osteoclastogenesis. Syn-1 has been reported to promote formation of multinucleated osteoclasts (30, 32), with most recent work suggesting that Syn-1 expression facilitates fusion between two multinucleated osteoclasts but not fusion between two mononucleated osteoclast precursors (30). A known ability of Syn-1 to mediate cell fusion (34) substantiated the hypothesis that Syn-1 involvement in osteoclastogenesis is related to its fusogenic activity. However, finding that the Syn-1-targeting reagent inhibits not only formation of multinucleated cells but also fusion-independent expression of TRAP (32) suggested that the Syn-1 role in osteoclastogenesis can be upstream of fusion. Furthermore, the RANKL-triggered osteoclastogenic differentiation is not accompanied by any significant up-regulation of either Syn-1 (Fig. S4) (32) or its receptor ASCT2 (32), and thus, if Syn-1 is indeed involved in osteoclast fusion, its activity has to be controlled.

Our results indicate that independently of possible contributions of Syn-1 upstream of fusion, this protein is directly involved in osteoclast fusion, and the results suggest that Syn-1 activity is regulated by other proteins identified in this study. We found the synchronized fusion between HM-derived OCPs to be strongly inhibited by reagents targeting either of these proteins and PS. Fig. 8*D* illustrates a suggested model for Syn-1 and Anx A5-dependent fusion downstream of the DC-STAMP-dependent PS externalization. Upon binding its receptors (Fig. 8*D,* not shown), Syn-1 trimer undergoes conformational changes that allow its fusion peptides to insert into the target membrane and to form a normally short-living extended conformation of the protein with exposed N-terminal heptad repeats and the C-terminal helices. In the normal fusion pathway (no LPC) and upon LPC removal in the synchronized fusion, formation of the extended conformation of the receptor-triggered Syn-1 facilitates an additional membrane-bridging mechanism provided by Anx-based complexes that assemble at the externalized PS and include S100A4 (50–53). This Anx-based bridging mechanism along with the final restructuring of Syn-1 into the lowest energy hairpin conformation pulls together and fuses the membranes (Fig. 8*D3*). In this model, fusion can be blocked both by Syn-1 peptide, which blocks the formation of the hairpin Syn-1 conformation, and by Anx A5 peptide, which blocks Anx A5-S100A4 binding.

Our findings suggest that, in contrast to fusion processes mediated by a single protein such as influenza virus fusion (54) and epithelial cell fusion in *C. elegans* (1), osteoclast fusion is controlled by a multiprotein fusion machinery. Multiprotein machinery also mediates vaccinia virus fusion (55) and SNARE-dependent intracellular fusion (56). Further research may expand the list of protein components of this machinery.

Defective osteoclast fusion could influence the bone integrity *in vivo*. Because large multinucleated osteoclasts resorb bones more efficiently than mononucleated TRAP-expressing osteoclasts, fusion between OCPs is considered significant for bone homeostasis (19, 20). Thus, although not all proteins essential for osteoclast formation are involved in fusion stage, we expect the components of the fusion machinery to contribute to the activity of osteoclasts *in vivo*. Indeed, DC-STAMP deficiency abrogates formation of multinucleated osteoclasts, increases bone mineral density and bone volume per tissue volume, and leads to mild osteopetrosis (21). Anx A1-deficient ($Anxa1^{tm1Rjf}$) male mice have a 25% higher bone mineral density than WT mice suggesting a mild osteopetrosis (57). Interestingly, Anx A1 deficiency did not change bone density in female mice. Anx A5 deficiency causes no gross differences in the appendicular skeleton in mice ($Anxa5^{tm1Epo}$) and has no effect on bone mineral density (58, 59). Syn-1 is not expressed in mice, where placentogenesis involves the other retrovirus-originated proteins syncytins A and B. Although BMCs from syncytin-B-deficient mice were found to be less efficient in forming multinucleated osteoclasts, the syncytin-B-deficient mice had no obvious bone phenotype (60).

The phenotypic manifestations of deficiencies in the fusion stage can be moderated by the redundancy of the contributions of different proteins and by the complex and dynamic feedback processes that regulate bone formation and remodeling. An example of this redundancy can be seen in OC-STAMP-deficient mice, which show normal bone resorption indicators and no evidence of bone abnormalities despite the lack of large multinucleated osteoclasts (24). It is likely that subtle effects of

fusion deficiencies can be better detected by studying the time courses of osteoclast formation and bone remodeling using approaches such as bone marrow ablation that induces new bone formation and resorption (61). This approach is comparable with inducing muscle regeneration to detect delayed myoblast fusion *in vivo* in Anx A1-deficient mice (17). Thus, additional studies are needed to elucidate not only the composition of the fusion machinery of osteoclasts but also the place and the role of osteoclast fusion in the tightly balanced bone remodeling processes in living animals. We expect that the fusion-synchronization approach applied here to uncouple membrane fusion from most of the pre-fusion differentiation processes will help in clarifying these questions and in the analysis of the intriguing heterogeneity of OCPs in osteoclast fusion (30, 62).

Mechanistic insights uncovered here for the cell–cell fusion stage of osteoclastogenesis, including the concerted action of Syn-1 and extracellular Anxs, assembled at the cell-surface PS, can be applicable to other cell–cell fusion processes. Indeed, diverse processes that involve cell fusions, including formation of multinucleated myotubes and giant inflammatory cells, fertilization, and formation of syncytiotrophoblasts in placentogenesis, are all accompanied by non-apoptotic exposure of PS (11, 13, 63, 64). Furthermore, myotube formation in skeletal muscle depends on Anxs A1 and A5 (7) and on Syn-1 (65, 66). Syn-1 (67), PS externalization (63, 68), and Anx A5 (69) also play major roles in formation of placental syncytium. To judge from these similarities, a concerted action of cell-surface PS-associated extracellular Anxs and endogenous retroviral envelope proteins can be a shared mechanistic motif for different cell–cell fusion processes.

To conclude, in this study, we uncoupled the cell fusion stage of osteoclastogenesis from the differentiation processes that prepare OCPs for fusion. We found that the merger of the membranes of human osteoclasts depends on DC-STAMP-regulated non-apoptotic externalization of PS, on PS-controlled assembly of extracellular PS-binding Anx A5 and Anx-binding S100A4, and on Syn-1. Better understanding of the specific contributions of the different components of the multiprotein machinery that controls osteoclast fusion as well as the effects of different deficiencies in this fusion process on bone homeostasis may help in developing new approaches to treating bone diseases.

Experimental procedures

Animals

All animal research followed the policies of the National Institutes of Health and USPHS and was approved by the Animal Care and Use Committee of the Eunice Kennedy Shriver NICHD. Primary bone marrow cells were isolated from 11-week-old female Anx A1 ($Anxa1^{tm1Rjf}$) (70) and Anx A5 ($Anxa5^{tm1Epo}$) knock-out mice (59) as well as from C57BL/6J wild-type mice purchased from The Jackson Laboratory. The mutant animals were in a C57BL/6J background.

Cells

Elutriated human monocytes from healthy donors were provided by the Department of Transfusion Medicine, National Institutes of Health. Cells were seeded at the density of 10^6 cells per 35-mm-diameter cell culture dish and cultured in the presence of MEM-α (Life Technologies, Inc.) supplemented with 10% (v/v) FBS and penicillin/streptomycin (complete medium). Cells were committed to osteoclast differentiation as described earlier (6). In brief, for the first 6 days, the cells were cultured in the medium supplemented with 25 ng/ml human M-CSF (Cell Sciences) and refreshed every 3rd day. Then the cells were incubated in the medium containing 25 ng/ml M-CSF and 30 ng/ml human RANKL (Cell Sciences) that was also refreshed every 3rd day. Murine macrophage-like RAW 264.7 cells (ATCC, Manassas, VA) (passage number $\leq$5) were maintained in 5% CO_2 at 37 °C in DMEM (Life Technologies, Inc.) supplemented with 10% (v/v) FBS (Valley Biomedical) and penicillin/streptomycin (Invitrogen). RAW cells were committed to osteoclastogenesis by culturing them in the medium supplemented with 50 ng/ml mouse RANKL (Cell Sciences) for 3–5 days. During the course of cell differentiation, the cells were replenished with RANKL-supplemented medium every 3rd day.

Primary murine BMCs were isolated from the femur and tibia of 11-week-old mice. Dissected bones were flushed using MEM-α (Life Technologies, Inc.) with no serum. To obtain single cell suspension, the cells were flushed using a syringe (HSW NORM-JECT Henke-Sass, Wolf GMBH) with a long 19-gauge needle and then 23- and 26-gauge needles (Covidien, MA). The cells were pelleted by centrifugation at 1600 rpm for 10 min at room temperature and resuspended in MEM-α supplemented with 10% FBS. The cell suspension was seeded and spread on a TC-treated cell culture dish (Falcon). After 3 h, the cell suspension was re-plated on a TC-treated cell culture dish overnight. Then, the cells were collected and centrifuged at 1400 rpm for 5 min at room temperature. Finally, the cell pellet was resuspended in 1 ml of MEM-α supplemented with 10% FBS. Cells were counted using an automated cell counter LUNA II™ (Logos Biosystem, Korea) and seeded at 500,000 cells per cm^2 or 165,000 cells per single well of a 96-well plate in the complete medium supplemented with 30 ng/ml murine-sRANKL (EMD, Millipore) and 20 ng/ml murine M-CSF (Cell Sciences). Medium was refreshed every 2nd day. 5 days after RANKL and M-CSF application, the cells were fixed with 10% (w/v) formalin solution (Electron Microscopy Sciences) and stained for TRAP, as described below.

Fusion synchronization using reversible LPC block

Osteoclast fusion was synchronized as described earlier (6). In brief, differentiating RAW cells at 72 h post-RANKL application were placed into the fresh culture medium containing 50 ng/ml murine RANKL and 170 μM lauroyl-LPC (1-lauroyl-2-hydroxy-*sn*-glycero-3-phosphocholine, Avanti Polar Lipids). Differentiating human monocytes at 72 h post-RANKL application (9th day post M-CSF application) were placed into the fresh culture medium containing 25 ng/ml human M-CSF, 30 ng/ml human RANKL, and, if not stated otherwise, 350 μM LPC. After 16 h LPC block was removed by five washes with LPC-free culture medium. If not stated otherwise, fusion was assayed 90 min later.

Syncytium formation and membrane merger assays

Osteoclast syncytium formation was scored as described earlier (6). In brief, to evaluate osteoclast fusion efficiency, the cells were fixed with 10% (w/v) formalin solution (Electron Microscopy Sciences). We labeled cell nuclei with Hoechst 33342 (Molecular Probes). In the case of osteoclasts generated from BMCs, the cells were fixed, and cell nuclei were labeled on the 5th day of cell culture. Images of the 10 randomly selected fields of view were captured at room temperature in Dulbecco's PBS (Life Technologies, Inc.) on an Axiovert 135 microscope (Carl Zeiss) equipped with ×10×/0.3 Plan Neofluar objective lens (Carl Zeiss) and Coolsnap fx CCD camera (Photometrics) using μManager 1.4 or on Axioskop microscope (Carl Zeiss) equipped with ×20/0.3 LD A-Plan objective lens (Carl Zeiss) and ORCA C4742-98 CCD camera (Hamamatsu Photonics) using MetaMorph 6.1 software (Molecular Devices). Osteoclast fusion efficiency was evaluated by counting the numbers of syncytia of different sizes (= number of nuclei per syncytium). The syncytia were defined either as cells with two or more nuclei for HM-derived and BMC-derived osteoclasts or as cells with three or more nuclei for RAW cell-derived osteoclasts (which tend to form much larger syncytia).

We quantified and presented the results as the total number of the cell fusion events required to generate the observed syncytia. The convenience of this new metrics is based on the fact that regardless of the sequence of fusion events (for instance, both for the case when only mononuclear OCPs fuse into syncytia and for the case when syncytia mostly grow by fusion between multinucleated cells), the number of cell-to-cell fusion events required to generate syncytium with N nuclei is always equal to $N - 1$. This expression can be easily proven by mathematical induction. Just to illustrate, a cell with four nuclei can be formed, for instance, by the following sequence: 1) formation of the first two-nucleated cell, *1 fusion event*; 2) formation of the second two-nucleated cell, *1 fusion event*; 3) fusion of two two-nucleated cells, *1 fusion event*. This sequence takes three fusion events, *i.e.* the same number of fusion events as formation of a four-nucleated cell by one-by-one fusion of four mononucleated cells (total of three fusion events).

We calculated the number of the cell fusion events required to generate the observed syncytia within the field of view as $\Sigma (N_i - 1) = N_{\text{total}} - N_{\text{syn}}$, where N_i is a number of nuclei in the individual syncytium; N_{total} is the total number of nuclei in syncytia, and N_{syn} is the number of syncytia. We normalized the number of fusion events to the total number of nuclei (including mononuclear cells) within the field. This quantification of the cell fusion events gives equal consideration to fusion between two mononucleated cells and fusion between two multinucleated cells. In contrast, the conventional ways of osteoclast fusion quantification as either the percentage of nuclei in syncytia or the number of multinucleated cells give different weight to fusion between mononucleated cells and fusion between multinucleated cells. Indeed, fusion between two multinucleated cells does not change the percentage of nuclei in syncytia, and it decreases rather than increases the number of syncytia.

The distributions of the sizes of syncytia under given conditions are presented as empirical CDF. In contrast to the frequently used histograms, CDF does not depend on arbitrary choice of bin size, allows direct reading of distribution median and quintiles from the graph, and is easier to compare between the different conditions. For HM- and BMC-derived osteoclasts, the number of nuclei and area of each multinucleated osteoclast (cells with ≥2 nuclei) were evaluated using semi-automated ImageJ (National Institutes of Health) macros developed in-house and available from L. V. C. on request.

Membrane merger (defined as formation of membrane connection between two cells that allows either lipid mixing or redistribution of cytosolic probes) was scored as described earlier (6). We labeled fusion committed OCPs labeled with different membrane and content probes. Because we aimed to separate membrane merger events (hemifusion and fusion pore opening) from post-fusion expansion of fusion pores to fully join volumes of two cells rather than to distinguish hemifusion (= only lipid mixing) from fusion pores (= both lipid and content mixing), we considered the appearance of any double-labeled cells as evidence of membrane merger.

RAW cells were labeled with either membrane probe dye DiI (Life Technologies, Inc.) or cell content marker Cell Tracker™ green 5-chloromethylfluorescein diacetate (CMFDA, "green cell tracker," Life Technologies, Inc.) at 72 h post-RANKL application. DiI-labeled cells were lifted and overlaid on top of green cell tracker-labeled cells. HMs were labeled with either green cell tracker or Cell Tracker™ orange CMRA dye ("orange cell tracker," Life Technologies, Inc.) at 72 h post-RANKL application. Orange cell tracker-labeled cells were lifted and overlaid on top of the green cell tracker-labeled cells. The co-plated differently labeled cells were incubated for 2 h in the RANKL-free medium to allow overlaid cells to settle down and then used in fusion-synchronization experiments as described above. In fusion between two mononucleated cells, treatments that do not affect membrane merger but inhibit fusion pore expansion are expected to result in appearance of mononucleated cells co-labeled with both dyes. Similarly, in fusion between two syncytia and in fusion between a mononucleated cell and a syncytium, the same treatments are expected to result in appearance of double-labeled syncytia without changing the number of syncytia. Because significant cell aggregation hinders unambiguous identification of mononucleated cells in our experimental system, we counted double-labeled syncytia and normalized the number of these syncytia to the total number of syncytia. If we inhibit only pore expansion, but not membrane merger (*i.e.* hemifusion plus non-expanding fusion pores), we expect that the number and sizes of syncytia will decrease, but local fusion of mononucleated cells to pre-existing differently labeled syncytia will result in the appearance of double-labeled syncytia. Indeed, that is what we previously observed after ATP depletion and dynamin 2 GTPase inhibition (6). If, however, membrane merger is inhibited, there will be no double-labeled syncytia. Thus, we interpret a decrease in the fraction of double-labeled syncytia as an indication of inhibition of early stages of fusion–fusion pore opening or hemifusion.

This quantification approach does not take into account membrane merger events between cells labeled with the same dye. However, within usual assumption that labeling does not affect fusion, the normalized extents of membrane merger presented in our study correctly represent the effects of different treatments on membrane merger.

Reagents

We used synthetic peptide inhibitor of Syn-1-mediated fusion (Syn-1 peptide, Ac-SGIVTEKVKEIRDRIQRRAEELRNTGPWGL-NH_2) described and characterized in Ref. 38 and, as a negative control (Syn-1 scr peptide), a peptide with the same amino acid composition but a scrambled sequence (Ac-GKWGLSRIRTELRNTEPVKEQVRAEIGDRI-NH_2). We also used Anx A1 and A5 peptides characterized in our earlier study (7). We used the peptide-mimicking N-terminal regions of human Anx A1 (Ac-^{2}AMVSEFLKQAWFIENEEQEYVQTVK^{26}-NH_2), the peptide with the same amino acid composition but a scrambled sequence (Ac-EMQSNAAVQYVEIKTWLEFEVKEQF-NH_2), and peptide mimicking the N-terminal region of human Anx A5 (Ac-^{2}AQVLRGTVTDFPGFDERAD^{20}-NH_2) and its scrambled version (Ac-LVATGGAVRPEDTFDRQDF-NH_2). All these peptides were custom-synthesized by GenScript. Calcium-activated chloride channel inhibitor CaCCinh-A01 ("A01") was purchased from EMD Millipore (Billerica, MA). Recombinant human lactadherin (MFGE8 recombinant protein) was purchased from MyBiosource (catalogue no. MBS1265312). Apoptotic cells were identified using either cell-impermeable probe TO-PRO®-3 iodide (Invitrogen, catalogue no. T3605) or CellEvent Caspase-3/7 green detection reagent (Thermo Fisher Scientific, catalogue no. C10723), as recommended by the manufacturers.

Fluorescence microscopy detection of PS, Syn-1, DC-STAMP, Anx A5, and S100A4 at the cell surface

In these experiments, we used non-permeabilized HM-derived OCPs or HM-derived macrophages at day 9 after placing them in M-CSF- and RANKL-supplemented medium or in only M-CSF-supplemented medium, respectively. Samples were imaged on Zeiss LSM510 confocal microscope, equipped with ×100/1.4 Oil Plan-Apochromat objective lens using appropriate optical setup. To detect cell-surface PS, we used either annexin V, Alexa Fluor® 488 conjugate (Thermo Fisher Scientific, catalogue no. A13201) or annexin 5 Alexa 647 conjugate (Invitrogen, catalogue no. A23204) applied to the cells in 1:20 dilution for 10 min at 37 °C. The amounts of the cell-surface PS were quantified using ×100 objective by measuring integrated fluorescence density per cell area with subtracted background integrated fluorescence density for more than 145 cells for each condition. To test the involvement of DC-STAMP in the PS exposure at the surface of fusion-committed HM-derived OCPs, antibody to DC-STAMP (EMD Millipore, MABF-39-1 clone 1A2 mouse monoclonal antibody MABF-39-1 clone 1A2) was applied at the time of LPC removal. PS exposure was quantified 2 h later.

To detect Syn-1, DC-STAMP, Anx A5, and S100A4 at the surface of the cells, we used as primary antibodies murine anti-ERVWE antibody (Abnova, catalogue no. H000308; 1:20 dilution), DC-STAMP (EMD Millipore, MABF-39-1 clone 1A2 mouse monoclonal antibody MABF-39-1 clone 1A2; 1:50), murine antibody to human Anx A5 (Abcam, catalogue no. ab54775; 1:20 dilution), and murine antibody to human S100A4 (LSBio, catalogue no. LS-C198143, 1:10 dilution), respectively. Human monocyte-derived cells were washed with PBS and fixed with warm (37 °C) 4% formaldehyde in PBS (Sigma, F1268). After three washes with PBS without calcium and magnesium, the cells were incubated in 10% FBS in PBS without calcium and magnesium to suppress non-specific binding. All primary antibodies were applied to the cells, still in 10% FBS in PBS without calcium and magnesium, for 1 h at room temperature. After five washes with PBS, the cells were incubated for 5 min with PBS, 10% FBS. Alexa Fluor 488-tagged goat anti-mouse antibodies (Thermo Fisher Scientific catalogue no. A-11001) were applied in PBS, 10% FBS in 1:400 dilution for 1 h at room temperature. To quantify Syn-1 expression at the surface of the 86 HM-derived macrophages and 33 HM-derived OCPs, we measured with ×100 objective the integrated fluorescence density per cell area. We then subtracted the background-integrated fluorescence density per cell area when the primary Syn-1 antibody was replaced with an antibody to adaptor protein fish (Santa Cruz Biotechnology, catalogue no. sc-376211). The amounts of the cell-surface Anx A5 were quantified for 150 HM-derived macrophages and 243 HM-derived OCPs by measuring with ×20 objective the integrated fluorescence density per cell area and subtracting the background integrated fluorescence density per cell area measured with fish antibody instead of specific primary antibodies. Cell-surface associated S100A4 was quantified using ×20 objective as the total fluorescence per field divided by the number of nuclei in the field (≥80 cells for each condition). In the experiments on cell-surface expression of DC-STAMP, Syn-1, Anx A5, and S100A4 presented in Fig. S4, we measured integrated fluorescence density per cell area for 40 cells for each condition in one experiment for each protein.

In co-localization experiments, we used rabbit antibodies to Anx A5 and murine antibodies to either Syn-1 or S100A4. After fixing the cells as described above, we applied 10 μl of FcR blocking solution in 100 μl of 10% FBS in PBS without calcium and magnesium for 10 min to suppress non-specific binding of rabbit antibodies. Then we applied primary antibodies (mouse antibody to one of the proteins and rabbit antibody to another in different combinations) in the same solution for 1 h at room temperature. After five washes with PBS, the cells were incubated for 5 min with PBS, 10% FBS. Alexa Fluor 488-tagged goat anti-mouse antibodies and Alexa Fluor 647-tagged goat anti-rabbit antibodies were applied in PBS, 10% FBS in 1:200 dilution for 1 h at room temperature.

Treatments

In our experiments on the effects of the different reagents on synchronized fusion, we used DC-STAMP antibody (5 μg/ml, Santa Cruz Biotechnology) or, when it became unavailable, DC-STAMP EMD Millipore MABF-39-1 clone 1A2 mouse monoclonal antibody. We also used Syn-1 antibody (35 μg/ml, rabbit antibody H-280 sc-50369, Santa Cruz Biotechnology). Syn-1 antibody application was preceded by a 5-min application of 10

μl of FcR blocking solution (Biolegends, catalogue no. 422301) in 2 ml of LPC-free medium. To verify the specificity of the used Syn-1 antibody, we transfected HeLa cells to express Syn-1 construct (71) and GFP and applied immunofluorescence microscopy using H-280 antibody as primary antibody.

S100A4 antibody (20 μg/ml, LSBio, catalogue no. LS-C198143, 1:10 dilution) was applied at the time of LPC removal. Fusion was assayed 1 h later. Rabbit polyclonal antibodies to Anx A1 Abcam catalogue no. ab65844) were applied to RAW cells and HM-derived OCPs at 5 and 35 μg/ml concentrations, respectively. Anx A2 polyclonal antibody (Santa Cruz Biotechnology, catalogue no. sc-9061) was applied to HM-derived OCPs either in 10 μg/ml concentration on day 9 of their differentiation with no LPC used or in 30 μg/ml concentration to the LPC-synchronized cells at the time of LPC removal. Rabbit Anx A5 antibody (5 μg/ml on RAW cells and 20 μg/ml on HM-derived osteoclast) or non-specific rabbit polyclonal IgG (5 μg/ml on RAW cells and 20 μg/ml on HM derived-osteoclast) were all purchased from Abcam (catalogue nos. ab14196 and ab37415, respectively). Antibody to myogenin (M-225) used in 35 μg/ml concentration as a negative control in Fig. 4*A* was purchased from Santa Cruz Biotechnology (catalogue no. sc-576). CD14 Ab was purchased from e-Bioscience (anti-mouse clone 13-0141-82) and used as a negative control in 20 μg/ml concentration. Mouse monoclonal antibody to RANK from Abcam (catalogue no. ab13918) was applied to HM-derived OCPs either in 2 μg/ml concentration on day 9 of the differentiation with no LPC used or in 20 μg/ml concentration to the LPC-synchronized cells at the time of LPC removal. Mouse monoclonal fish (G-7) antibody (Santa Cruz Biotechnology, catalogue no. sc-376211) was used as a negative control for RANK antibody.

We also used lactadherin or A01 (120 μM), Syn-1 peptide (20 μg/ml), or Anx peptides (100 μg/ml). If not stated otherwise, all reagents were applied immediately after washing the cells with LPC-free culture medium.

TRAP staining

Osteoclast cell differentiation marker TRAP was labeled using TRAP staining kit (Kamiya Biomedical Co.) and evaluated as described earlier (6). In short, several random fields of view were imaged on an Axiovert 135 microscope (Carl Zeiss) equipped with ×10/0.30 Plan-NEOFLUAR objective lens (Carl Zeiss), EGFP/FITC/Cy2/Alexa Fluor 488 filter set and Coolsnap fx CCD camera (Photometrics) using μManager 1.4. To quantify TRAP staining, TRAP-positive areas were automatically selected using an IJ-Isodata threshold that was followed by morphological dilation and fill holes operations. Thus, the obtained binary mask was applied to the inverted bright field image, and total pixel intensity of the final image was measured.

Bone resorption assay

Bone resorption activity was determined according to the manufacturer's protocol using Corning Osteo Assay Surface 24-well multiple plates. In brief, human monocytes seeded at a density of 200,000 cells/well were committed to osteoclastogenesis, as described earlier. In the control experiment, the cells underwent uninterrupted differentiation (no LPC). In the fusion-synchronization experiment, on day 8 of the differentiation (2 days post-RANKL application), the cells were placed into fresh culture medium containing 25 ng/ml human M-CSF, 30 ng/ml human RANKL, and 210 μM LPC. LPC block was lifted 16 h later by washing the cells with LPC-free medium. Note that the concentration of LPC used in these experiments was selected to effectively synchronize fusion in the 24-well plates used in the resorption assay. Both in the control experiment and in the fusion-synchronization experiment, on day 11 of the differentiation (5 days post-RANKL application) and, in the case of the fusion-synchronization experiment, 48 h post-LPC wash, the cells were removed by incubation with 10% (v/v) bleach solution (Sigma; catalogue no. 425044) for 5 min at room temperature. The plates were washed with distilled water to remove the bleach solution and dried completely at room temperature. Images were captured on AxioObserver D1 (Zeiss) microscope equipped with ×10/0.45 Plan Apochromat (Zeiss) objective lens and edge5.5 CMOS camera (PCO) using Micromanager 1.4.22 software. To quantify the bone-resorbed area, images were processed using a median filter and automatically thresholded using an Yen's algorithm in ImageJ.

Statistics and data presentation

Each set of experiments for each graph presented here was repeated on at least three occasions with similar results. Presented data were averaged from the same set of experiments. We prepared graphs and performed statistical analyses using Sigmaplot version 13.0 (Systat Software). The data are presented as *box plots* and *bar charts* with individual experimental points shown. Normally distributed data were analyzed using the unpaired Student's *t* test. When the data were not normally distributed or failed the equal variance test, we used the Mann-Whitney rank sum test instead.

Author contributions—S. K. V. performed all functional experiments. E. L. carried out all immunofluorescence experiments and phosphatidylserine exposure detection. K. M. designed approaches used to quantify fusion by image analysis. C. G. managed the mouse colony and euthanized the animals for *ex vivo* experiments. M. F. Y. and V. K. provided intellectual support on bone biology implications of the results. B. U. contributed to the discussions of the data. S. K. V., E. L., K. M., and L. V. C. designed experiments and analyzed data. L. V. C. and S. K. V. wrote the paper with contributions from all coauthors.

Acknowledgments—We thank Dr. LiQi Li for advice on the experiments on isolation of the murine bone marrow cells and Dr. Karl Pfeifer for the kind support of our work. The Anx A5 knock-out mice were generously provided by Drs. Ernst Pöschl and Bent Brachvogel.

References

1. Jahn, R., Lang, T., and Südhof, T. C. (2003) Membrane fusion. *Cell* **112,** 519–533 CrossRef Medline
2. Martens, S., and McMahon, H. T. (2008) Mechanisms of membrane fusion: disparate players and common principles. *Nat. Rev. Mol. Cell Biol.* **9,** 543–556 CrossRef Medline
3. Podbilewicz, B. (2014) Virus and cell fusion mechanisms. *Annu. Rev. Cell Dev. Biol.* **30,** 111–139 CrossRef Medline
4. White, J. M., and Whittaker, G. R. (2016) Fusion of enveloped viruses in endosomes. *Traffic* **17,** 593–614 CrossRef Medline

5. Chen, E. H., Grote, E., Mohler, W., and Vignery, A. (2007) Cell–cell fusion. *FEBS Lett.* **581,** 2181–2193 CrossRef Medline
6. Verma, S. K., Leikina, E., Melikov, K., and Chernomordik, L. V. (2014) Late stages of the synchronized macrophage fusion in osteoclast formation depend on dynamin. *Biochem. J.* **464,** 293–300 CrossRef Medline
7. Leikina, E., Melikov, K., Sanyal, S., Verma, S. K., Eun, B., Gebert, C., Pfeifer, K., Lizunov, V. A., Kozlov, M. M., and Chernomordik, L. V. (2013) Extracellular annexins and dynamin are important for sequential steps in myoblast fusion. *J. Cell Biol.* **200,** 109–123 CrossRef Medline
8. Ciechonska, M., and Duncan, R. (2014) Reovirus FAST proteins: virus-encoded cellular fusogens. *Trends Microbiol.* **22,** 715–724 CrossRef Medline
9. Chernomordik, L. V., and Kozlov, M. M. (2003) Protein-lipid interplay in fusion and fission of biological membranes. *Annu. Rev. Biochem.* **72,** 175–207 CrossRef Medline
10. Podbilewicz, B., Leikina, E., Sapir, A., Valansi, C., Suissa, M., Shemer, G., and Chernomordik, L. V. (2006) The *C. elegans* developmental fusogen EFF-1 mediates homotypic fusion in heterologous cells and *in vivo*. *Dev. Cell* **11,** 471–481 CrossRef Medline
11. Helming, L., and Gordon, S. (2009) Molecular mediators of macrophage fusion. *Trends Cell Biol.* **19,** 514–522 CrossRef Medline
12. van den Eijnde, S. M., van den Hoff, M. J., Reutelingsperger, C. P., van Heerde, W. L., Henfling, M. E., Vermeij-Keers, C., Schutte, B., Borgers, M., and Ramaekers, F. C. (2001) Transient expression of phosphatidylserine at cell-cell contact areas is required for myotube formation. *J. Cell Sci.* **114,** 3631–3642 Medline
13. Lyden, T. W., Ng, A. K., and Rote, N. S. (1993) Modulation of phosphatidylserine epitope expression by BeWo cells during forskolin treatment. *Placenta* **14,** 177–186 CrossRef Medline
14. Hochreiter-Hufford, A. E., Lee, C. S., Kinchen, J. M., Sokolowski, J. D., Arandjelovic, S., Call, J. A., Klibanov, A. L., Yan, Z., Mandell, J. W., and Ravichandran, K. S. (2013) Phosphatidylserine receptor BAI1 and apoptotic cells as new promoters of myoblast fusion. *Nature* **497,** 263–267 CrossRef Medline
15. Wu, Z., Ma, H. M., Kukita, T., Nakanishi, Y., and Nakanishi, H. (2010) Phosphatidylserine-containing liposomes inhibit the differentiation of osteoclasts and trabecular bone loss. *J. Immunol.* **184,** 3191–3201 CrossRef Medline
16. Bizzarro, V., Fontanella, B., Franceschelli, S., Pirozzi, M., Christian, H., Parente, L., and Petrella, A. (2010) Role of annexin A1 in mouse myoblast cell differentiation. *J. Cell. Physiol.* **224,** 757–765 CrossRef Medline
17. Leikina, E., Defour, A., Melikov, K., Van der Meulen, J. H., Nagaraju, K., Bhuvanendran, S., Gebert, C., Pfeifer, K., Chernomordik, L. V., and Jaiswal, J. K. (2015) Annexin A1 deficiency does not affect myofiber repair but delays regeneration of injured muscles. *Sci. Rep.* **5,** 18246 Medline
18. Park, S. Y., Yun, Y., Lim, J. S., Kim, M. J., Kim, S. Y., Kim, J. E., and Kim, I. S. (2016) Stabilin-2 modulates the efficiency of myoblast fusion during myogenic differentiation and muscle regeneration. *Nat. Commun.* **7,** 10871 CrossRef Medline
19. Vignery, A. (2008) Macrophage fusion: molecular mechanisms. *Methods Mol. Biol.* **475,** 149–161 CrossRef Medline
20. Miyamoto, T. (2011) Regulators of osteoclast differentiation and cell–cell fusion. *Keio J. Med.* **60,** 101–105 CrossRef Medline
21. Yagi, M., Miyamoto, T., Sawatani, Y., Iwamoto, K., Hosogane, N., Fujita, N., Morita, K., Ninomiya, K., Suzuki, T., Miyamoto, K., Oike, Y., Takeya, M., Toyama, Y., and Suda, T. (2005) DC-STAMP is essential for cell–cell fusion in osteoclasts and foreign body giant cells. *J. Exp. Med.* **202,** 345–351 CrossRef Medline
22. Chiu, Y. H., and Ritchlin, C. T. (2016) DC-STAMP: a key regulator in osteoclast differentiation. *J. Cell. Physiol.* **231,** 2402–2407 CrossRef Medline
23. Miyamoto, H., Suzuki, T., Miyauchi, Y., Iwasaki, R., Kobayashi, T., Sato, Y., Miyamoto, K., Hoshi, H., Hashimoto, K., Yoshida, S., Hao, W., Mori, T., Kanagawa, H., Katsuyama, E., Fujie, A., *et al.* (2012) Osteoclast stimulatory transmembrane protein and dendritic cell-specific transmembrane protein cooperatively modulate cell–cell fusion to form osteoclasts and foreign body giant cells. *J. Bone Miner. Res.* **27,** 1289–1297 CrossRef Medline
24. Witwicka, H., Hwang, S. Y., Reyes-Gutierrez, P., Jia, H., Odgren, P. E., Donahue, L. R., Birnbaum, M. J., and Odgren, P. R. (2015) Studies of OC-STAMP in osteoclast fusion: a new knockout mouse model, rescue of cell fusion, and transmembrane topology. *PLoS ONE* **10,** e0128275 CrossRef Medline
25. Pellegatti, P., Falzoni, S., Donvito, G., Lemaire, I., and Di Virgilio, F. (2011) P2X7 receptor drives osteoclast fusion by increasing the extracellular adenosine concentration. *FASEB J.* **25,** 1264–1274 CrossRef Medline
26. Erlandsson, M. C., Svensson, M. D., Jonsson, I. M., Bian, L., Ambartsumian, N., Andersson, S., Peng, Z., Vääräniemi, J., Ohlsson, C., Andersson, K. M. E., and Bokarewa, M. I. (2013) Expression of metastasin S100A4 is essential for bone resorption and regulates osteoclast function. *Biochim. Biophys. Acta* **1833,** 2653–2663 CrossRef Medline
27. Rhee, I., Davidson, D., Souza, C. M., Vacher, J., and Veillette, A. (2013) Macrophage fusion is controlled by the cytoplasmic protein tyrosine phosphatase PTP-PEST/PTPN12. *Mol. Cell. Biol.* **33,** 2458–2469 CrossRef Medline
28. Oikawa, T., Oyama, M., Kozuka-Hata, H., Uehara, S., Udagawa, N., Saya, H., and Matsuo, K. (2012) Tks5-dependent formation of circumferential podosomes/invadopodia mediates cell–cell fusion. *J. Cell Biol.* **197,** 553–568 CrossRef Medline
29. Kang, H., Kerloc'h, A., Rotival, M., Xu, X., Zhang, Q., D'Souza, Z., Kim, M., Scholz, J. C., Ko, J. H., Srivastava, P. K., Genzen, J. R., Cui, W., Aitman, T. J., Game, L., Melvin, J. E., *et al.* (2014) Kcnn4 is a regulator of macrophage multinucleation in bone homeostasis and inflammatory disease. *Cell Rep.* **8,** 1210–1224 CrossRef Medline
30. Møller, A. M., Delaissé, J. M., and Søe, K. (2017) Osteoclast fusion: time-lapse reveals involvement of CD47 and syncytin-1 at different stages of nuclearity. *J. Cell. Physiol.* **232,** 1396–1403 CrossRef Medline
31. Shin, N. Y., Choi, H., Neff, L., Wu, Y., Saito, H., Ferguson, S. M., De Camilli, P., and Baron, R. (2014) Dynamin and endocytosis are required for the fusion of osteoclasts and myoblasts. *J. Cell Biol.* **207,** 73–89 CrossRef Medline
32. Søe, K., Andersen, T. L., Hobolt-Pedersen, A. S., Bjerregaard, B., Larsson, L. I., and Delaissé, J. M. (2011) Involvement of human endogenous retroviral syncytin-1 in human osteoclast fusion. *Bone* **48,** 837–846 CrossRef Medline
33. Hobolt-Pedersen, A. S., Delaissé, J. M., and Søe, K. (2014) Osteoclast fusion is based on heterogeneity between fusion partners. *Calcif. Tissue Int.* **95,** 73–82 CrossRef Medline
34. Mi, S., Lee, X., Li, X., Veldman, G. M., Finnerty, H., Racie, L., LaVallie, E., Tang, X. Y., Edouard, P., Howes, S., Keith, J. C., Jr, and McCoy, J. M. (2000) Syncytin is a captive retroviral envelope protein involved in human placental morphogenesis. *Nature* **403,** 785–789 CrossRef Medline
35. Antony, J. M., Ellestad, K. K., Hammond, R., Imaizumi, K., Mallet, F., Warren, K. G., and Power, C. (2007) The human endogenous retrovirus envelope glycoprotein, syncytin-1, regulates neuroinflammation and its receptor expression in multiple sclerosis: a role for endoplasmic reticulum chaperones in astrocytes. *J. Immunol.* **179,** 1210–1224 CrossRef Medline
36. Menaa, C., Devlin, R. D., Reddy, S. V., Gazitt, Y., Choi, S. J., and Roodman, G. D. (1999) Annexin II increases osteoclast formation by stimulating the proliferation of osteoclast precursors in human marrow cultures. *J. Clin. Invest.* **103,** 1605–1613 CrossRef Medline
37. Li, F., Chung, H., Reddy, S. V., Lu, G., Kurihara, N., Zhao, A. Z., and Roodman, G. D. (2005) Annexin II stimulates RANKL expression through MAPK. *J. Bone Miner. Res.* **20,** 1161–1167 CrossRef Medline
38. Chang, C., Chen, P. T., Chang, G. D., Huang, C. J., and Chen, H. (2004) Functional characterization of the placental fusogenic membrane protein syncytin. *Biol. Reprod.* **71,** 1956–1962 CrossRef Medline
39. Suzuki, J., Fujii, T., Imao, T., Ishihara, K., Kuba, H., and Nagata, S. (2013) Calcium-dependent phospholipid scramblase activity of TMEM16 family members. *J. Biol. Chem.*
40. Zaitseva, E., Zaitsev, E., Melikov, K., Arakelyan, A., Marin, M., Villasmil, R., Margolis, L. B., Melikyan, G. B., and Chernomordik, L. V. (2017) Fusion stage of HIV-1 entry depends on virus-induced cell surface exposure of phosphatidylserine. *Cell Host Microbe* **22,** 99–110.e7 CrossRef Medline
41. Otzen, D. E., Blans, K., Wang, H., Gilbert, G. E., and Rasmussen, J. T. (2012) Lactadherin binds to phosphatidylserine-containing vesicles in a

two-step mechanism sensitive to vesicle size and composition. *Biochim. Biophys. Acta* **1818,** 1019–1027 CrossRef Medline
42. Lizarbe, M. A., Barrasa, J. I., Olmo, N., Gavilanes, F., and Turnay, J. (2013) Annexin-phospholipid interactions. Functional implications. *Int. J. Mol. Sci.* **14,** 2652–2683 CrossRef Medline
43. Mah, S. J., Lee, J., Kim, H., Kang, Y. G., Baek, S. H., Kim, H. H., and Lim, W. H. (2015) Induction of S100A4 in periodontal ligament cells enhances osteoclast formation. *Arch. Oral. Biol.* **60,** 1215–1221 CrossRef Medline
44. van Genderen, H. O., Kenis, H., Hofstra, L., Narula, J., and Reutelingsperger, C. P. (2008) Extracellular annexin A5: functions of phosphatidylserine-binding and two-dimensional crystallization. *Biochim. Biophys. Acta* **1783,** 953–963 CrossRef Medline
45. Richard, J. P., Leikina, E., Langen, R., Henne, W. M., Popova, M., Balla, T., McMahon, H. T., Kozlov, M. M., and Chernomordik, L. V. (2011) Intracellular curvature-generating proteins in cell-to-cell fusion. *Biochem. J.* **440,** 185–193 CrossRef Medline
46. Markosyan, R. M., Miao, C., Zheng, Y. M., Melikyan, G. B., Liu, S. L., and Cohen, F. S. (2016) Induction of cell–cell fusion by Ebola virus glycoprotein: low pH is not a trigger. *PLoS Pathog.* **12,** e1005373 CrossRef Medline
47. Hwang, S. Y., and Putney, J. W., Jr. (2011) Calcium signaling in osteoclasts. *Biochim. Biophys. Acta* **1813,** 979–983 CrossRef Medline
48. Chen, X., Doffek, K., Sugg, S. L., and Shilyansky, J. (2004) Phosphatidylserine regulates the maturation of human dendritic cells. *J. Immunol.* **173,** 2985–2994 CrossRef Medline
49. Youn, M. Y., Fujiyama-Nakamura, S., Takada, I., Imai, Y., and Kato, S. (2010) Identification of osteoclastic factors in the nuclear envelope of mature, multinucleated osteoclasts. *Biosci. Biotechnol. Biochem.* **74,** 1956–1959 CrossRef Medline
50. König, J., Prenen, J., Nilius, B., and Gerke, V. (1998) The annexin II-p11 complex is involved in regulated exocytosis in bovine pulmonary artery endothelial cells. *J. Biol. Chem.* **273,** 19679–19684 CrossRef Medline
51. Santamaria-Kisiel, L., Rintala-Dempsey, A. C., and Shaw, G. S. (2006) Calcium-dependent and -independent interactions of the S100 protein family. *Biochem. J.* **396,** 201–214 CrossRef Medline
52. Myrvang, H. K., Guo, X., Li, C., and Dekker, L. V. (2013) Protein interactions between surface annexin A2 and S100A10 mediate adhesion of breast cancer cells to microvascular endothelial cells. *FEBS Lett.* **587,** 3210–3215 CrossRef Medline
53. Eden, E. R., Sanchez-Heras, E., Tsapara, A., Sobota, A., Levine, T. P., and Futter, C. E. (2016) Annexin A1 tethers membrane contact sites that mediate ER to endosome cholesterol transport. *Dev. Cell* **37,** 473–483 CrossRef Medline
54. Hamilton, B. S., Whittaker, G. R., and Daniel, S. (2012) Influenza virus-mediated membrane fusion: determinants of hemagglutinin fusogenic activity and experimental approaches for assessing virus fusion. *Viruses* **4,** 1144–1168 CrossRef Medline
55. Moss, B. (2016) Membrane fusion during poxvirus entry. *Semin. Cell Dev. Biol.* **60,** 89–96 CrossRef Medline
56. Rizo, J., and Xu, J. (2015) The synaptic vesicle release machinery. *Annu. Rev. Biophys.* **44,** 339–367 CrossRef Medline
57. Damazo, A. S., Moradi-Bidhendi, N., Oliani, S. M., and Flower, R. J. (2007) Role of annexin 1 gene expression in mouse craniofacial bone development. *Birth Defects Res. A Clin. Mol. Teratol.* **79,** 524–532 CrossRef Medline
58. Belluoccio, D., Grskovic, I., Niehoff, A., Schlötzer-Schrehardt, U., Rosenbaum, S., Etich, J., Frie, C., Pausch, F., Moss, S. E., Pöschl, E., Bateman, J. F., and Brachvogel, B. (2010) Deficiency of annexins A5 and A6 induces complex changes in the transcriptome of growth plate cartilage but does not inhibit the induction of mineralization. *J. Bone Miner. Res.* **25,** 141–153 CrossRef Medline
59. Brachvogel, B., Dikschas, J., Moch, H., Welzel, H., von der Mark, K., Hofmann, C., and Pöschl, E. (2003) Annexin A5 is not essential for skeletal development. *Mol. Cell. Biol.* **23,** 2907–2913 CrossRef Medline
60. Coudert, A., Redelsperger, F., Chabbi-Achengli, Y., Marty, C., Decrouy, X., Dupressoir, A., Heidmann, T., and de Vernejoul, M.-C. (2015) in *The 4th Joint Meeting of European Calcified Tissue Society and the International Bone and Mineral Society, Rotterdam, The Netherlands, April 25–28, 2015,* p. 194, ECTS-IBMS Abstracts, Rotterdam, The Netherlands
61. Chen, X. D., Allen, M. R., Bloomfield, S., Xu, T., and Young, M. (2003) Biglycan-deficient mice have delayed osteogenesis after marrow ablation. *Calcif. Tissue Int.* **72,** 577–582 CrossRef Medline
62. Levaot, N., Ottolenghi, A., Mann, M., Guterman-Ram, G., Kam, Z., and Geiger, B. (2015) Osteoclast fusion is initiated by a small subset of RANKL-stimulated monocyte progenitors, which can fuse to RANKL-unstimulated progenitors. *Bone* **79,** 21–28 CrossRef Medline
63. Das, M., Xu, B., Lin, L., Chakrabarti, S., Shivaswamy, V., and Rote, N. S. (2004) Phosphatidylserine efflux and intercellular fusion in a BeWo model of human villous cytotrophoblast. *Placenta* **25,** 396–407 CrossRef Medline
64. Curia, C. A., Ernesto, J. I., Stein, P., Busso, D., Schultz, R. M., Cuasnicu, P. S., and Cohen, D. J. (2013) Fertilization induces a transient exposure of phosphatidylserine in mouse eggs. *PLoS ONE* **8,** e71995 CrossRef Medline
65. Bjerregard, B., Ziomkiewicz, I., Schulz, A., and Larsson, L. I. (2014) Syncytin-1 in differentiating human myoblasts: relationship to caveolin-3 and myogenin. *Cell Tissue Res.* **357,** 355–362 CrossRef Medline
66. Frese, S., Ruebner, M., Suhr, F., Konou, T. M., Tappe, K. A., Toigo, M., Jung, H. H., Henke, C., Steigleder, R., Strissel, P. L., Huebner, H., Beckmann, M. W., van der Keylen, P., Schoser, B., Schiffer, T., *et al.* (2015) Long-term endurance exercise in humans stimulates cell fusion of myoblasts along with fusogenic endogenous retroviral genes *in vivo*. *PLoS ONE* **10,** e0132099 CrossRef Medline
67. Frendo, J. L., Olivier, D., Cheynet, V., Blond, J. L., Bouton, O., Vidaud, M., Rabreau, M., Evain-Brion, D., and Mallet, F. (2003) Direct involvement of HERV-W Env glycoprotein in human trophoblast cell fusion and differentiation. *Mol. Cell. Biol.* **23,** 3566–3574 CrossRef Medline
68. Adler, R. R., Ng, A. K., and Rote, N. S. (1995) Monoclonal antiphosphatidylserine antibody inhibits intercellular fusion of the choriocarcinoma line, JAR. *Biol. Reprod.* **53,** 905–910 CrossRef Medline
69. Degrelle, S. A., Gerbaud, P., Leconte, L., Ferreira, F., and Pidoux, G. (2017) Annexin-A5 organized in 2D-network at the plasmalemma eases human trophoblast fusion. *Sci. Rep.* **7,** 4217 CrossRef
70. Hannon, R., Croxtall, J. D., Getting, S. J., Roviezzo, F., Yona, S., Paul-Clark, M. J., Gavins, F. N., Perretti, M., Morris, J. F., Buckingham, J. C., and Flower, R. J. (2003) Aberrant inflammation and resistance to glucocorticoids in annexin 1−/− mouse. *FASEB J.* **17,** 253–255 Medline
71. Chuprin, A., Gal, H., Biron-Shental, T., Biran, A., Amiel, A., Rozenblatt, S., and Krizhanovsky, V. (2013) Cell fusion induced by ERVWE1 or measles virus causes cellular senescence. *Genes Dev.* **27,** 2356–2366 CrossRef Medline